



Analysing the Characteristics of Neural Networks for the Recognition of Sugar Beets

Applied University of Hamm-Lippstadt

Bachelor thesis
for the attainment of the academic degree
Bachelor of Engineering

submitted by
Luca Brodo

Electronic Engineering
Mat.Nr.: 2180015
luca.brodo@stud.hshl.de

25. Februar 2022

First supervisor: Prof. Dr. Stefan Henkler
Second supervisor: Prof. Dr. Achim Rettberg
Second supervisor: Dipl.-Wirt.-Inf. Kristian Rother

Affidavit

I, Luca Brodo, herewith declare that I have composed the present paper and work by myself and without use of any other than the cited sources and aids. Sentences or parts of sentences quoted literally are marked as such; other references with regard to the statement and scope are indicated by full details of the publications concerned. The paper and work in the same or similar form has not been submitted to any examination body and has not been published.

Lippstadt, 25. Februar 2022

Luca Brodo

Sugar beets plantations are perfect candidates for the application of smart farming methodologies. While bringing innumerable benefits, most of the proposed solutions are based on the recognition of the plants to increase yield and increase sustainability of the plantation. As the recognition task is usually tackled using Convolutional Neural Networks (CNNs), the unpredictability of them imposes great challenges to engineers. In this paper, we focus on the analysis of the networks to find correlations between their characteristics to be reliable and predictable in time, with the aim of making sugar beet recognition more transparent. We will start our investigation from defining and analysing the characteristics we are interested in. This step allows us to find appropriate techniques to create a benchmark tool for the analysis neural networks. We will use this tool and the characteristics we define to investigate the training and inference process of eight models using two different dataset.

Although these two use cases show promising results, as we are only going to focus on analysing models and finding correlations between some of their characteristics, this paper is only the first milestone towards using this correlation to optimize smart farming applications to improve the production and sustainability of the plantations around the world.

Table of Content

1 Motivation	13
1.1 Smart Farming in Sugar Beet Plantations	14
1.2 Organization of the Paper	15
2 Related Work	17
3 Characteristics of Neural Networks	21
3.1 Deep Neural Networks and Uncertainty	21
3.2 Learning Process and Training Time	25
3.3 Inference Time	26
3.4 Accuracy	27
3.5 Precision and Recall	28
3.6 Loss	29
3.7 Overfitting and Underfitting	30
3.8 Architecture	32
3.8.1 Alexnet	32
3.8.2 VGG Networks	33
3.8.3 Residual Neural Networks	33
4 Analysing the Models	37
4.1 Benchmarking	37
4.1.1 Key Characteristics for a Correct Benchmark	38
4.1.2 Benchmark Techniques and Methodologies	39
4.1.3 Common Practices in Benchmarking	42
4.2 Benchmarking Deep Neural Networks	43
4.2.1 Benchmark Inference Time	43
4.2.2 Benchmark Training Time	48
4.2.3 Measuring Accuracy	48
4.3 Benchmarking Tool for Neural Networks	49
4.3.1 Analysing the Training Process	51
4.3.2 Analysing inference Time	52
4.3.3 Further Analysis	54
5 Analysis of the characteristics	55
5.1 Test Environment	55
5.2 Fist Experiment	56
5.3 Second Experiment	64
6 Overview and Future Work	75

References	77
A Appendix	87

List of Figures

1.1	Depiction of a sugar beet plant	14
3.1	Trend in publications about Deep Learning	21
3.2	Differences between how DNNs and humans recognize objects	23
3.3	Illustrating the difference between aleatoric and epistemic uncertainty	24
3.4	Validation and training loss curve	30
3.5	Real example of the validation error curve	31
3.6	Real-world example of the validation and training loss curve	32
3.7	Overview of the architecture of Alexnet	33
3.8	Overview of the various architectures for VGG	34
3.9	Residual learning: a building block	34
3.10	Overview of the Resnet architecture	35
4.1	This snippet of code shows an example of use of the function <i>clock()</i>	40
4.2	Synopsis of the command <i>time</i>	40
4.3	Program used to test the command <i>time</i>	41
4.4	Command to disable turbo boost in both AMD and Intel devices	42
4.5	Command to disable Hyper-Threading	43
4.6	Command to set the scaling governor policy to be <i>performance</i> for every CPU	43
4.7	Imprecise way to benchmark for inference time	44
4.8	More precise way to measure inference time	45
4.9	Method to benchmark on Android with Tensorflow Lite	45
4.10	Command to access the measured inference time in Tensorflow-Lite	45
4.11	Architecture of the convolutional neural network used as an example to calculate inference time	47
4.12	Benchmark for training time using the watchdog approach	49
4.13	Function in fast.ai that calculates the accuracy	49
4.14	Behaviour of the benchmarking suite on a conceptual level	49
4.15	Example of graphs produced by the tool when analysing training time	52
4.16	Example of the graphs produced by the tool when analysing inference time	52
4.17	Overview of the process to test inference	53
5.1	Accuracy achieved by the models after being trained for 100 epochs	57
5.2	Accuracy achieved when training for 100 epochs in relation with training time	58
5.3	Training loss and validation loss of all models calculated over 100 epochs .	58
5.4	Training loss and validation loss of Resnet101 and Resnet152 over 100 epochs	59
5.5	Inference time measured for each model	60
5.6	Inference time measured for Resnet101 and Resnet152	61
5.7	Size of the images over inference time for the seedlings dataset	62

5.8	Training loss and validation loss of Resnet101 and Resnet152 over 100 epochs on the 'plant_seedlings_v2' dataset and the grey-scale variant of the pictures	63
5.9	Inference time of each model trained with grey images as well	64
5.10	Accuracy achieved by the models over 50 epochs	65
5.11	Accuracy achieved by the models during the training phase plot over training time	65
5.12	Accuracy of Alexnet and Resnet152 against training time in seconds	66
5.13	Accuracy of Resnet101 and VGG9 against training time in seconds	66
5.14	Breaking point of Resnet101 and VGG19	67
5.15	Accuracy achieved by the models over 10 epochs	68
5.16	Accuracy achieved by the models over 100 epochs	69
5.17	Training loss and validation loss of all models calculated over 100 epochs	69
5.18	Inference time measured for each model	70
5.19	Inference time measured for models Resnet18 and Alexnet	70
5.20	Size of the images over inference time	71
5.21	Inference time of the slowest images for models VGG16 and Resnet152	72
5.22	Inference time of the slowest images for models Resnet18 and Alexnet	72
A.1	Histogram of the slowest files in common amongst all models	87
A.2	Example of the architecture of residual networks	88
A.3	Histogram of the fastest files of Resnet 152	89
A.4	Histogram of the slowest files of Resnet152	90
A.5	Complete result of the test for inference time in the seedlings dataset	91
A.6	Complete result of the test for inference time in the seedlings dataset with grey images	92
A.7	Complete result of the test for inference time in the seedlings dataset with grey images. The inference here is calculated by feeding grey scale images to the models	93

List of Tables

2.1	Comparison between the three different approaches using AlexNet	17
2.2	Comparison between the classification performance of different Neural Networks	18
3.1	Example for binary classification	27
4.1	Metrics obtained from the fast.ai <i>fit_one_cycle()</i> function	48
4.2	Example of training time results	51
5.1	Specifics of the machine which run the experiments	55
5.2	Categories of the 'plant_seedlings_v2' dataset	56
5.3	Performances of the models trained with the 'plant_seedlings_v2' dataset for 100 epochs	57
5.4	Difference between validation loss and train loss after 100 epochs	59
5.5	Performance of the models trained for 100 epochs on the 'plant_seedlings_v2' dataset including the grey-scale variant of the pictures	62
5.6	Difference between validation loss and train loss after 100 epochs using the gray-scale variants of the pictures	63
5.7	Average time for each epoch	68
5.8	Information collected from the slowest pictures	73

1 Motivation

The seemingly unstoppable growth of global population compounded by climate change is putting an enormous pressure on the agricultural sector. As estimated by the World Resources Institutes (WRI), the number of people on our planet will reach an astounding 10 billion by 2050 ([AAUS⁺19]) and, as a result, the agricultural production must double to keep up with the demand [SGSS16]. However, the agricultural sector is facing immense challenges due to plant diseases, pests and weed infestation and in these times, like never before, the switch to a more sustainable model seems inevitable. The main target of sustainable farming is to increase yield while reducing reliance on herbicides and pesticides, and therefore trying to target treatments only to plants that specifically require it by monitoring key indicators of each individual crop, a technique usually referred to as "precision farming". This technique is notoriously time and energy consuming, if done manually, and therefore usually discarded in favour of more traditional methodologies [LHS⁺16a].

In the last years there has been, however, an increased focus on integrating cutting-edge technology with precision farming to improve quality and quantity of agricultural production, while at the same time lowering the inputs - like manual labour - significantly [IRP⁺21]. This system is also known as "smart farming" and it is based on the adoption of autonomous robots, which could be both wheeled robots and Unmanned Aerial Vehicles (UAVs), and it has been enabled by the astonishing advancements in the field of the Internet of Things (IoT).

IoT is the key technology behind smart farming and allows to add value to the data collected by automated processes by ensuring data flow between different devices [IRP⁺21]. More importantly, IoT allows more cost-efficient and timely production and management practices, as showed by Glaroudis et al. in [GIC20], and at the same time, the reduction of the inherent climate impact by enabling real-time reactions to infestations, such as weed, pest or diseases, and by enabling a more adequate use of resources such as water, pesticides or agro-chemicals [IRP⁺21]. In other words, IoT makes precision farming not only more efficient in terms of both money and resources, but even more sustainable than other traditional farming methods.

One of the cultivations which will benefit immensely by the adoption of smart farming is the sugar beet. The *Beta vulgaris L.*, depicted in Fig. 1.1, commonly referred to as sugar beet, is ranked as the second most cultivated sugar crop all over the world next to sugarcane [BP20]. As showed by May in [May03], being a slow-growing crop early in the season [BP20], this plant seems to be a very poor competitor against weed, a claim also backed up by Schweizer's researches, which reports that sugar beet root yields can be reduced by 26–100% by uncontrolled weed growth. [SD89]



Fig. 1.1: Depiction of a sugar beet plant [Mas91]

1.1 Smart Farming in Sugar Beet Plantations

An approach based on smart farming could reduce the effect of weed infestations on sugar beet plantations and increment the yield and the sustainability of said plantation.

As a matter of fact, even though tractors and hand labour are still vastly used for weed management, since the 50s herbicides have been the most used method of weed management in sugar beets farms ([CM10]) and, apart from the well known environmental damage which the use herbicides leads to, another implication is the effect that they have on the sugar beet crops themselves. Most of the 'selective' herbicides have influence on sugar beet growth, with early symptoms showing on the leaves, which can, in all possibility, reduce the yield. [Pet04]

To optimize and remove the effects of pesticides, the new frontier for weed management is to automatize the more traditional mechanical techniques ([RNSF20], [FMF⁺14], [MPSG21]). Mechanical techniques, and even techniques which use selective spraying of herbicides, however, require that the sugar beet is localized before they can be applied to avoid ruining the plantation. In the research field, a lot of proposed solutions employ Convolutional Neural Networks (CNNs) for recognition tasks ([GFP⁺20], [SIHvH18], [RAMP20], [MLS17], [NWH21]).

CNNs, however, impose great challenges to the developers. For example, in real time applications, classification time is of the highest importance since it affects the ability to respect deadlines. Furthermore, the performance of CNNs is influenced by many factors, like for e.g. training time or the data-set used for training.

Being able to predict the performances of CNNs before their deployment will allow engineers to precisely model the application to tailor them for the CNN of their choice.

In this paper, we are going to investigate whether it is possible to make those predictions by empirically studying some of the metrics which can influence CNNs' performances and find correlations amongst them in order to be able to be precise, scalable and predictable in time. As the result of our investigation, we aim to develop a toolbox for the employment of CNNs in sugar beet recognition.

1.2 Organization of the Paper

In order to achieve the aforementioned goal, we will first analyse the main characteristics of CNNs in chapter number 3. This will allow us to lay out the foundations for our further studies, since it is essential to have a proper grounding of what can influence the recognition of sugar beets.

Subsequently, in chapter number 4, we will study how we can benchmark CNNs to obtain the measurements we need to find the correlations. Benchmarking is a notoriously convoluted task, however at the end of our study, we will be able to create a tool to measure performances and analyse CNNs in a precise and reproducible way.

Finally, with the help of our tool, in chapter 5 we will profile CNNs with fairly different architectures to identify correlations between their metrics so that we will be able to optimize the recognition of sugar beets.

2 Related Work

Multiple proposed solutions in the academia for sugar beet recognition use Convolutional Neural Networks (CNNs) to recognize both weed and sugar beets in a plantation. The solutions we are going to consider have been studied more thoroughly in [Luc22].

Gao et al. in [GFP⁺20] developed a CNN based on the popular tiny YOLOv3 framework ([ARK20]), but with modifications for increased performances. They added two more layers for better feature fusion and reduced the number of detection to two, rather than the standard three for YOLO, since the images of sugar beets they collected were generally similar in size.

Instead of using only images collected from the field, the authors developed a tool to synthetically generate over 2000 images of sugar beets, which, according to them, allowed them to save time and resources. The model they developed has an accuracy of ~83% with an average inference time of 6.48ms.

Suh et al. in [SIHvH18] focused their study on the Alexnet architecture (section 3.8.1) considering three approaches: AlexNet as a fixed feature extractor, modified and fine-tuned AlexNet as a binary classifier, modified and fine-tuned AlexNet as a fixed feature extractor. An overview of the three approaches can be seen in table 2.1.

Approach	Highest accuracy	Training time (s)	Classification time (s)	# of Images
1	97%	13.3	0.016	1100
2	98.0%	656.4	0.012	900
3	96.7%	195.8	0.0130s	300
3	97.3%	581.4	0.0130s	800

Table 2.1: Comparison between the three different approaches using AlexNet [SIHvH18]

Authors of [SIHvH18] also provide a comparison between six fine-tuned deep networks, namely AlexNet, VGG-19, GoogLeNet, ResNet-50, ResNet-101 and Inception-v3, summarized in table 2.2.

Both table 2.1 and 2.2 show how differently NNs perform in similar settings when some metrics are changed. For example, in table 2.2, we can see that both Resnet50 and Resnet101 achieve different inference time when trained for different numbers of epochs, i.e. with different training time.

Regarding the study of Neural Network performances, both academic and industrial organizations have already developed numerous benchmark solutions to evaluate the behaviour of NNs under different workloads and on different devices. For example, authors of [LHZ⁺20] and [ITK⁺19] have proposed benchmarks of NNs specifically for mobile devices. *Hendrycks et al.* in [HD19] developed a benchmark to assess the robustness of image classifiers under condition of perturbations.

Network	Accuracy	Training time	Classification time
20 Epoch			
AlexNet	97.9%	9.0min	0.0038s
VGG-19	98.4%	37.4min	0.0130s
GoogLeNet	97.0%	23.8min	0.0033s
ResNet-50	96.2%	40.3min	0.0072s
ResNet-101	97.5%	106.6min	0.0118s
Inception-v3	90.8%	88.7min	0.0088s
30 Epoch			
AlexNet	97.7%	15.6min	0.0040s
VGG-19	98.7%	71.4min	0.0124s
GoogLeNet	97.3%	36.9min	0.0035s
ResNet-50	97.2%	69.8min	0.0075s
ResNet-101	98.5%	162.0min	0.0111s
Inception-v3	94.8%	133.0min	0.0086s

Table 2.2: Comparison between the classification performance of different Neural Networks [SIHvH18]

Reddi et al. in [RCK⁺20] propose a benchmark, namely MLPerf, to evaluate inference of Machine Learning system under various workloads. They divided workloads under high level tasks, such as image classification, and they provide a reference model for it.

Zou et al. in [ZAZ⁺18], among other contributions, proposed a benchmark suite to analyse NNs' training time of eight different state-of-the-art models under six different application domains. The metrics they collect during profiling are:

Throughput

Throughput is defined as the amount of input samples processed by the networks. This metric is relevant because, contrary to inference, it is not latency sensitive.

GPU utilization

They define the GPU utilization as the fraction of time in which the GPU is busy, it is calculated as follows:

$$\text{GPU Utilization} = \frac{\text{GPU Active Time} \times 100}{\text{total elapsed time}} \quad (2.1)$$

FP32 utilization

This metric refers to the percentage of floating operations done during training, since typically training DNNs is performed using single precision floating point operations (FP32). This metric measures how effectively the GPU resources are used. It is calculated as:

$$\text{FP32 Utilization} = \frac{\text{actual flop counting during } T \times 100}{\text{FLOPS}_{\text{peak}} \times T} \quad (2.2)$$

Where:

- $FLOPS_{peak}$ is the GPU theoretical peak analysis
- T is the period of time in seconds that the GPU is active

CPU utilization

This is calculated as the average utilization of each CPU core:

$$\frac{\sum_c \text{total time of active core } c \times 100}{\text{CPU core count} \times \text{total elapsed time}} \quad (2.3)$$

Memory consumption

The memory consumed by the NNs during training

Although the aforementioned benchmarks have brought many advancements to the field, they are not meant to be used to study the characteristics of the NNs, but rather to compare and assess NNs performance under different conditions and workloads. Therefore, in future parts of this paper, we will explore techniques to measure NNs performance and determine their behaviour for our own specific goal and under our conditions.

3 Characteristics of Neural Networks

In this chapter, we will explore the characteristics of NN models we want to measure and analyse. For the rest of the paper, we will use the term *characteristics* to identify all the metrics and properties of NNs which will have an influence on their performances during an actual deployment. The term is, therefore, an umbrella term for any type of measurable property which can influence the recognition of sugar beets. In the following sections we will give a thorough overview of each one of them, with the main goal of understanding them.

3.1 Deep Neural Networks and Uncertainty

As the scope of our investigation is to be able to recognize characteristics and find empirically their correlations in the field of sugar beet recognition, we need to be able to produce predictable and reliable results in order to present the foundations for our analysis. Although this is true in general terms, before we explore techniques to measure Neural Networks, it is important that we understand that we can not properly use the term "predictability" when discussing DNNs.

Due to the increased trust given by the advancements in recent years, DNNs are being applied in numerous different fields, as shown by the increasing number of peer review papers about Deep Learning (Fig. 3.1), even in high-risk applications like medical image analysis or autonomous vehicle control. [GTA⁺21]

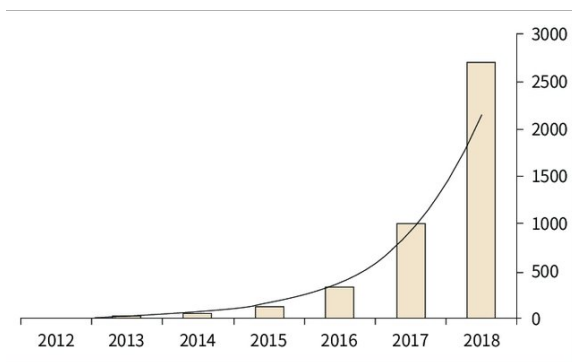


Fig. 3.1: Trend in publications about Deep Learning [SKD19]

In such high-risk scenarios, DNNs should not only be highly accurate, as a mistake in detecting an obstacle could cause catastrophic consequences for the passengers, but also be trustworthy enough so that the probability of the predicted values reflects the ground truth. DNNs, however, are subjected to different sources of uncertainty and errors. *Galiwoski et al.* in [GTA⁺21] recognized five crucial factors which can cause uncertainty and errors in

DNNs.

Those factors are:

- I. The variability in real world situations.
- II. The errors inherent to the measurement systems.
- III. The errors in the architecture specification of the DNN.
- IV. The errors in the training procedure of the DNN.
- V. The errors caused by unknown data.

We can model a neural network as a function f , parametrized by weight θ , which maps a set of input \mathbb{X} to a set of measurable outputs \mathbb{Y} , hence:

$$f\theta : \mathbb{X} \rightarrow \mathbb{Y} \quad f\theta(x) = y \quad (3.1)$$

In case of supervised learning, we also model the training set as $\mathcal{D} \subset \mathbb{D} = \mathbb{X} \times \mathbb{Y}$, where \mathbb{X} is an instance space and \mathbb{Y} the set of outcomes that can be associated with an instance ([HW21]), containing N samples. A DNN trained in \mathcal{D} can therefore predict a corresponding target $f\theta(x^*) = y^*$.

During the data acquisition process, a measurement x and a target variable y are taken from space Ω to represent a real world situation ω . For example, ω could be a sugar beet, y the label "sugar beet" and x a picture of a sugar beet. The job of the DNN is therefore to predict the label from the image of the sugar beet (Eq n. 3.1). In a real world situation, however, measurements could be potentially different from the ones used for training and this could influence the prediction of y . The source of this difference could be different lighting conditions, different environmental conditions or any other general conditions not taken into account when training. A new measurement generally is not part of the training set, hence $x^* \notin \mathcal{D}$. These differences in real world scenarios compared to the training set are called *distribution shifts* ([OFR⁺19]) and DNN are very sensitive to that. Moreover, sources of noise could also be identified in errors in labelling. This is the first factor that can cause uncertainty, i.e. **the variability in real world situations**. [GTA⁺21]

In addition, it has to be taken into account that measurement devices are also subjected to noise due to defects or imprecision. This kind of noise is the second factor, i.e. **the errors inherent to the measurement systems**. [GTA⁺21]

We previously modelled a neural network simply as a function $f\theta$. Although in most applications DNN are treated similarly to how we modelled them, i.e. as a black box which takes as input some data and outputs a prediction, they have a certain structure with certain parameters to take care of. These parameters can be for example the amount of layers, the parameters which need to be configured and the chosen activation function. These configurations are up to the modeller and are the third cause of uncertainty in DNNs, i.e. **the errors in the architecture specification of the DNN**. [GTA⁺21]

A further source of uncertainty in DNNs is also related to the very nature of DNNs themselves. DNNs are not deterministic, rather they are stochastic¹ in many ways: the order of data, the weight initialization or random regularization as augmentation or dropout [GTA⁺21]. Moreover, the stochastic gradient descent algorithm is widely used to optimize the learning process of DNNs. [Rud17]

¹Stochastic is a synonym for randomness

Another version of the gradient descent algorithm is the mini-batch version, which selects random batches with aleatory size (called batch size) from the learning data-set to optimize the training process. [Rud17] This parameter, in addition to other ones like learning rate, and the number of training epochs, is also source of unpredictability in the DNN, as they could heavily change its performances

The stochastic nature of DNNs and the choices of the aforementioned parameters are the forth cause of uncertainty in DNNs : **the errors in the training procedure of the DNN**

Previously we modelled the training set as $\mathcal{D} \subset \mathbb{D}$, hence as being a subset of a certain domain \mathbb{D} . However, the realm of input which could be fed to a neural network is not limited to this domain, rather the DNN is trained to solve tasks with inputs belonging to this domain. Another source of uncertainty can be therefore an input which the DNN is not trained for, even though it is able to process it. For instance, if a DNN is trained to classify dogs from images, an image as input could also depict a bird. The last factor which could cause uncertainty is therefore the **errors caused by unknown data**. Such unknown data could also be caused by highly noisy measurement devices, like a broken camera, and some researches show how easy it is to fool DNNs with images that are meaningless for us humans [NYC15]. Fig.3.2 depicts some examples of pictures which could fool even the most advanced DNN. The figures on the top row could also be produced by random noise from a malfunctioning camera and yet could be classified as something else with an accuracy $\geq 99.6\%$. [NYC15]

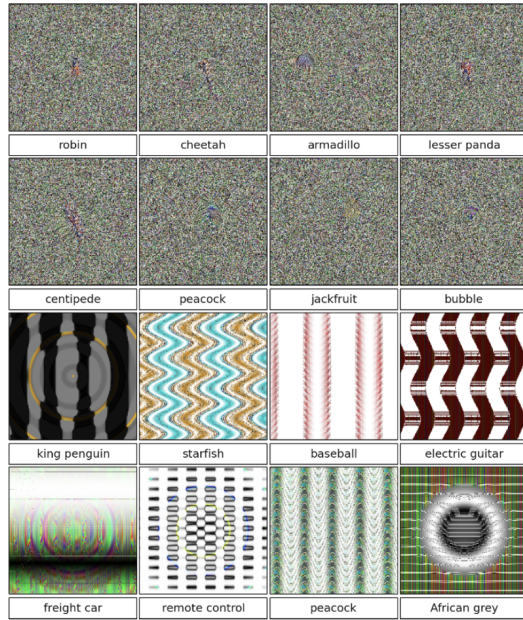


Fig. 3.2: This result highlights differences between how DNNs and humans recognize objects. Images are either directly (top) or indirectly (bottom) encoded [NYC15]

With the help of the five factors we studied before, we can further categorize uncertainty in two main categories: aleatoric and epistemic uncertainty. [HSHK21]

Aleatoric uncertainty is also usually referred to as data or statistical uncertainty, and it is generally used to identify the type of uncertainty causes by the nature of randomness,

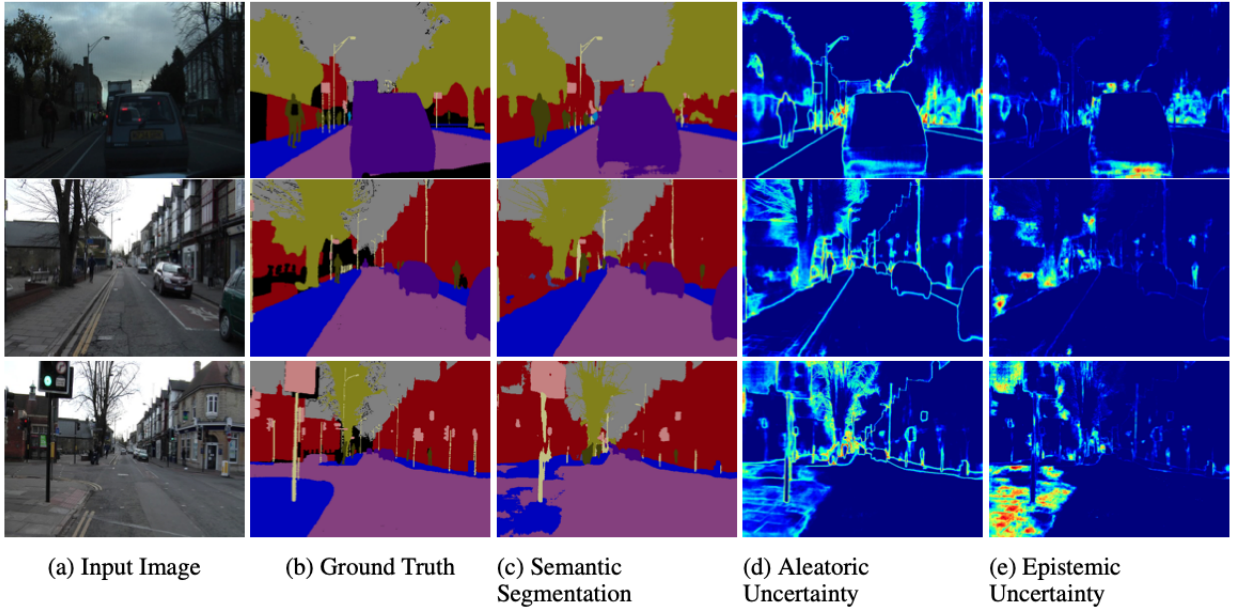


Fig. 3.3: Illustrating the difference between aleatoric and epistemic uncertainty for semantic segmentation on the CamVid dataset [BC18]

that is *the variability in the outcome of an experiment which is due to inherently random effects* [HSHK21]. Moreover, it also comprises the type of noise directly stemming from the noise in data used to train, validate, and test for inference performance, therefore referring to factor II [GTA⁺21] [BC18].

Aleatoric uncertainty is of the irreducible type, meaning it is impossible to get rid of. ([KG17], [HSHK21]) For example, a model that predicts the output of a flip coin, even in case of a perfect model, is not able to produce the definite, correct answer for it, but only a prediction of the possibilities for the two outcomes. This is due to the fact that the data used for this model is of random, stochastic nature and this random component can not be reduced. [HSHK21]

Epistemic uncertainty, or systemic uncertainty, on the other hand, refers to the type of uncertainty caused by ignorance or shortcomings of the model, hence not on any other underlying stochastic phenomenon [BC18]. Usually, this is due to unknown or lack of coverage of the dataset used for training, hence covers factors I, III, IV and V.

Epistemic uncertainty can be theoretically explained away by improving the architecture of the model and broadening the dataset. For example, let us consider a model which is able to determine whether a word is part of the Italian or English dictionary. If we feed the word "macchina" to the model, given that we provided enough data to train and the model is perfect, we can be confident that it will predict the correct language, in this case Italian. However, if we feed it with the word "pasta", we can not be confident that the prediction is correct, i.e. we can only obtain the probability of this word to be part of one of the dictionaries **given the dataset we provided**. As a matter of fact, the word "pasta" is present in both dictionaries and the outcome depends on the probability of the word to appear in one of the dictionaries in our dataset. The first case it is clear case of epistemic uncertainty, which we were able to completely remove with a perfect dataset; while the latter is a clear case of aleatoric uncertainty and it is impossible to remove. Fig. 3.3 helps visualize the difference between the two. In pictures (d), we can see that the aleatoric

uncertainty increases on object boundaries and objects far from the camera. Pictures (*e*), on the other hand, shows how epistemic uncertainty increases for semantically and visually challenging pixels. For example, the bottom row shows a failure case when the model fails to segment the footpath due to high epistemic uncertainty, but low aleatoric uncertainty. [KG17]

Although this distinction is very helpful for further and more precise analysis on a DNN model, it is also important to note that the distinction between the two is highly dependent on the context: they are not absolute notions ([KD09]). Hence, changing the settings of the model will blur the distinction line between the two and therefore make their classification considerably more difficult. [HSHK21]

We mentioned previously that theoretically model uncertainty is 100% reducible. However, in the case of real world data this is not the case. In addition to the probabilistic nature of the DNNs, the training dataset used for the model is very likely to be only a subset of all possible input data of the application, hence it is also very likely that unknown data for the domain is unavoidable. In addition, the exact representation of the uncertainty of the DNN is not possible, as the different sources of uncertainty can not be generally modelled accurately. [GTA⁺21]

For the purpose of this paper, we are not going to explore methodologies to reduce this uncertainty, nor are we going to investigate any further whether this uncertainty can be predicted from other properties. Our goal will be to research whether we will be able to correlate the other metrics in a way that we are able to be predictable in time, meaning whether we are able to define time frames for training or inference based on the other characteristics we are going to define.

3.2 Learning Process and Training Time

Training time, as the name implies, is the time required to train a Neural Network, or any machine learning model to perform a specific task. *Mitchell* in [Mit97] provides a general definition for the training, or learning, process: “*A computer program is said to learn from experience E with respect to some class of tasks T and performance measure P, if its performance at tasks in T, as measured by P, improves with experience E*”. This definition is quite broad ([GBC16]) and it is out of the scope of this paper to give a formal definition for the experience E, task T, and performance measure P.

When it comes to Neural Networks, the process of training is the process of updating the weights of the network so that the network is able to achieve the desired goal. [Mur16] The network weights are updated during back propagation by the following equation ([Mur16]):

$$W = W_{old} - \eta \frac{dE}{dW_{old}} \quad (3.2)$$

Equation 3.2 implies that the new value for the weights W is obtained by the difference between the old value W_{old} and the gradient of W_{old} of the error function E multiplied by the learning rate η . The learning rate is a tuning parameter that determines the step size at each iteration while moving towards a minimum of the error function, as we are moving opposite to the gradient. The error, or ”scoring”, function can be defined as the

sum of squared differences between the network's output (equation n. 3.3) and the correct output and it is applicable when the output is a vector, matrix, or tensor of continuous real values ([Mur16]).

$$E(W, b) = \frac{1}{N} \sum_{i=1}^N \frac{1}{2} \|h_{W,b}(x^{(i)}) - y^{(i)}\|^2 \quad (3.3)$$

Equation 3.3 refers to the Mean Squared Error (MSE), a type of error function usually applied to regression problems and it estimates the average squared difference between the actual values $y^{(i)}$ and the predicted values $h_{W,b}(x^{(i)})$. In other types of problems, different error functions are used. We will describe error functions later in the paper.

The learning experience can be broadly categorized into two main categories: supervised and unsupervised learning. Roughly speaking, given a dataset \mathcal{D} , an unsupervised learning algorithm aims to learn useful properties of this dataset. In the context of deep learning, we aim to learn the entire probability distribution $p(\mathcal{D})$ that generated the dataset or some useful properties of it. On the other hand, supervised learning implies the use of a dataset \mathcal{D} and an associated value or label \mathbb{Y} to teach the model to predict \mathbb{Y} from $\mathbb{X} \subset \mathcal{D}$, usually by estimating the conditional probability $p(\mathbb{Y}|\mathbb{X})$ ([Mur16]).

Usually the learning process proceeds in waves of mini-batches, which allow to avoid both over-fitting and under utilization of GPU's compute parallelism. [ZAZ⁺18]

Finally, the learning process is a memory demanding task, as backward pass and weight updates - operations unique to training - need to save intermediate results in GPU memory (in some cases tens of gigabytes are required). [RGC⁺16]

Training time is an often overlooked metrics of Neural Networks compared to inference (3.3) or accuracy (3.4) ([ZAZ⁺18]), however, due to the recent growth in applications of Deep Learning technologies in various fields ([BTD⁺16], [HWT⁺15], [10.16], [AAB⁺15b]) training time is acquiring more attention. [ZAZ⁺18]

3.3 Inference Time

In Machine Learning, therefore in Deep Learning as well, the term "inference time" is used to indicate the time required for the trained model to make predictions, regardless of the correctness of said predictions.

Inference time has attracted a lot of attention in the research field, since executing already trained Neural Networks efficiently is inarguably a still open problem. ([ZAZ⁺18], [MTK⁺17], [DHH⁺18], [TMK16])

Differently from training time (section 3.2), the memory footprint for inference is in the order of Mega-Bytes ([HLM⁺16]). As a matter of fact, inference is latency sensitive, but computationally less demanding. [ZAZ⁺18]

3.4 Accuracy

Accuracy is usually one of the most looked after metrics when analysing Neural Network performances ([HD19], [BCCN18]). Accuracy is usually the factor taken into account when the training process is evaluated, as it could be a potential factor deciding when to stop the training. Being able to predict accuracy, for example, could help detect, and therefore terminate, unsuccessful training runs. [UKG⁺21]

Usually, the term "accuracy" refers to the *classification accuracy* of the neural network. The classification accuracy is the ratio of the number of correct predictions to the total number of input samples ([HW20]) and it is calculated with equation n. 3.4.

$$\text{Accuracy} = \frac{\text{Number of correct predictions}}{\text{Total number of predictions}} \quad (3.4)$$

In case of a multi-class prediction problem, however, classification accuracy is meaningful only when each class contains an equal number of samples. For example, considering two classes *A* and *B* containing 98% and 2% of the samples respectively, the model can reach 98% accuracy by predicting exclusively samples from class *A*.

Another definition which is often used for accuracy in Neural Networks in the context of *binary classification* is the one shown in equation n. 3.5.

$$\text{Accuracy} = \frac{TP + TN}{TP + TN + FP + FN} \quad (3.5)$$

Where TP = True Positives, TN = True Negatives, FP = False Positives, and FN = False Negatives. This equation defines accuracy as the proportion between correctly predicted values (true positives and true negatives) and the sum of all predictions, regardless of their correctness.

Similarly to classification accuracy, however, this definition could be misleading as well. For example, considering a model that classified 100 tumors as malignant (the positive class) or benign (the negative class) as shown in table 3.1.

TP	FP	FN	TN
1	1	8	90

Table 3.1: Example for binary classification

Calculating the accuracy using equation n. 3.5. will give an accuracy of :

$$\text{Accuracy} = \frac{1 + 90}{1 + 90 + 1 + 80} = 0.91 \quad (3.6)$$

At first glance, this metric would show that the model is performing correctly (91 correct out of a 100). The dataset is composed of 91 tumors that are benign (90 TNs and 1 FP) and 9 that are malignant (1 TP and 8 FNs). The model is able to identify 90 out of 91 benign tumors correctly, but only 1 out of 9 as malignant. This is another case of class-imbalanced data sets in which a model that would only classify tumors as benign would reach the same level of accuracy. [Goo10]

3.5 Precision and Recall

As we already delineated in section number 3.4, sometimes analysing only based on accuracy might be misleading, especially when we are dealing with class-imbalanced data-sets. Accuracy does not distinguish between the number of correct labels of different classes [SJS06]. In these cases, two other metrics we can observe are *precision* and *recall*. Formally, *precision* is defined as equation n. 3.7 and it represents the number of detected anomalies that are actual real anomalies [TLZ⁺19]. In other words, it expresses the proportion of positive identifications that was correct over the number of correct predictions.

$$\text{Precision} = \frac{TP}{TP + FP} \quad (3.7)$$

Where TP = True Positives and FP = False Positives.

On the other hand, *recall* is defined as equation n. 3.8 and it represents the number of real anomalies that have been detected. [TLZ⁺19]

$$\text{Recall} = \frac{TP}{TP + FN} \quad (3.8)$$

Where TP = True Positives and FN = False Negatives.

It is calculated, therefore, as the proportion of positive predictions that were correct over the correct positive predictions and the incorrect negative identifications.

We can use the example in table 3.1 to calculate both precision and recall.

$$\begin{aligned} \text{Precision} &= \frac{TP}{TP + FP} \\ &= \frac{1}{1 + 1} \\ &= \frac{1}{2} \\ &= 0.5 \end{aligned} \quad (3.9)$$

Having a precision of 0.5, our model is correct 50% of the time when it predicts that a tumor is malignant.

$$\begin{aligned} \text{Recall} &= \frac{TP}{TP + FN} \\ &= \frac{1}{1 + 8} \\ &= \frac{1}{9} \\ &= 0.11 \end{aligned} \quad (3.10)$$

In other words, with a recall of 0.11, our model has been able to identify 11% of all malignant tumors.

Ideally, we would like to have a high recall percentage as well as a high precision one. Unfortunately, this is rarely the case since improving recall often comes at the expense of precision, since in order to increase the TP for the minority class, the number of FP is also often increased, resulting in reduced precision. [HM13]

Furthermore, as it was the case for accuracy, neither precision nor recall give a full insight

on the performance of the model, since a model could have high precision with low recall, as shown in the example above. It is, therefore, common practice to combine both with a weighted harmonic mean as an F score [vR74]:

$$F_\beta = (1 + \beta^2) \frac{Precision * Recall}{\beta^2 * Precision + Recall} \quad (3.11)$$

In equation n. 3.11, the coefficient β represents the balance between precision and recall, with high values favouring recall. Usually, the F-score is used with $\beta = 1$, so a perfect balance between precision and recall, and in this case it is called F1 score (Equation n. 3.12). [Der16]

$$F1 = (2) \frac{Precision * Recall}{Precision + Recall} \quad (3.12)$$

When evaluating the F score, however, the focus is given exclusively to true positives, false positives and false negatives, neglecting the true negative group, which is usually the majority class. In addition, using only the F score, one is unable to distinguish low-recall from low-precision systems. [Der16]

3.6 Loss

When training a Neural Network, finding the perfect weights for the neurons is impossible, therefore the problem is usually modelled as an optimization problem. As an optimization problem, it is solved using an algorithm which aims to optimize the weights to make good predictions. Usually, Neural Networks are trained using the Stochastic Gradient Descent (SGD) and the weights are updated through back-propagation. In the context of an optimization algorithm, the function which evaluates a candidate solution is defined as the objective function and such function in Neural Networks evaluates how good a prediction is, hence the SGD is used to minimize this function, i.e. finding the solution with the lowest score. When we are minimizing the objective function, we are referring to it as the cost function, loss function, or error function. [GBC16]

The loss function has the fundamental job of faithfully distilling all the aspects of the model, both good and bad, down into a single scalar value, which allows candidate solutions to be compared. [RM99]

The choice of the loss function is highly influenced by the output layer of the Neural Network. The output layer defines the type of the solution we defined for the problem, i.e. if it is a regression problem or a classification problem. In other words, the way we represent the output determines the loss function. [GBC16]

The following are some of the best practices for each type of problem.

Regression problem

For this type of problems, usually the output layer is one node with a linear activation unit, therefore the loss function to use is the Mean Squared Error(MSE).

Binary Classification problem

The output layer is one node with a sigmoid activation unit and the loss function used is Cross-Entropy, or Logarithmic loss.

Multi-class Classification problem

The output layer is composed of one node for each class using the soft-max activation function and the loss function used is Cross-Entropy, or Logarithmic loss.

3.7 Overfitting and Underfitting

As we already discovered in section n. 3.2, the training routine is necessary for the model in order to make predictions on a new set of data. Therefore, the goal of the learning process is not to maximize the accuracy on the training set, but rather to maximize its predictive accuracy on the new data points. [Die95]

If the model works too hard to find the best fit for the training data there is the risk that it is going to fit the noise present on the data-set, hence it will learn the inevitable peculiarities and bias present in the training set, rather than finding a general predictive rule. In other words, the performance of the model will decrease when tested against an unknown data-set. [JK15]

This phenomenon is called *over-fitting*. [Die95]

Over fitting is influenced by the training data fed to the model, as small data-sets are more prone to it, even though large data-sets can also be affected. [DSSM09]

Under fitting, on the other hand, can be considered as the opposite process. This occurs when the model is too simple for the training data and it is incapable of learning the variability of the data. [DSSM09]

One strategy to avoid over fitting is to use a so-called "early-stopping" approach. This approach consists simply of stopping the training before over-fitting can occur and it is one of the most commonly used strategies to avoid this phenomena, as it is simple to understand and proven to be the superior one in many cases. ([FHZ93], [Pre00])

The key part of this approach is to divide the training set into two parts, namely the validation set and the training set, and to use those to find a criteria to stop the training process.

Fig. 3.4 shows the idealized evolution over time of the error on the training set and on a validation set not used for training, i.e. training and validation loss. [Pre00]

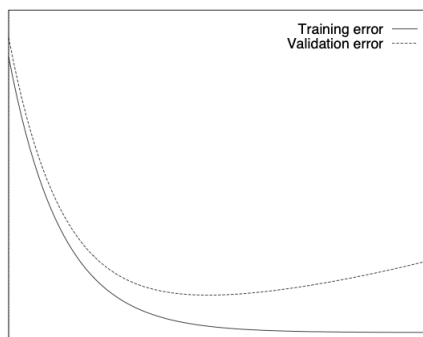


Fig. 3.4: Validation and training loss curve. The x axis is time, the y axis is the loss [Pre00]

Following the trend in Fig. 3.4, we can observe that the validation error decreases until a certain point together with the training loss before increasing indefinitely. We can use the validation error to approximate the generalization error and, therefore, stop the

training in the moment where the validation loss is increasing again. We can summarize the "early-stopping" approach in the following steps:

1. Split the training data into a training set and a validation set, for e.g. in a 4-to-1 proportion.
2. Train over the training and evaluate the validation loss every arbitrary number of epoch.
3. Stop training as so on as the error on the validation set is higher than it was last time.
4. Use the weights the network had in that previous step as the result of the training run.

Furthermore, depending on the data, there might also be situations in which the validation loss is not constantly bigger than the training loss, as shown in Fig. 3.4. As a matter of fact, this graph shows an idealized behaviour of the two curves. A real example for this curve can be seen in Fig. 3.5.

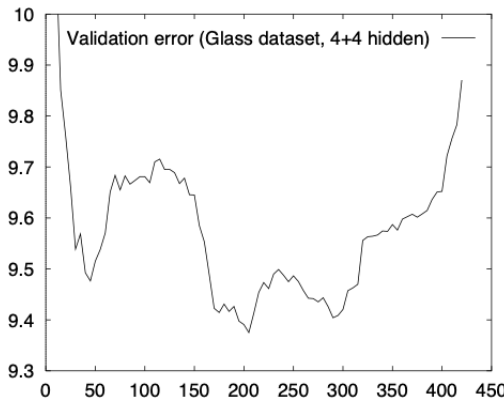


Fig. 3.5: Real example of the validation error curve. The x axis is time, the y axis is the error [Pre00]

In such situations, it would be particularly difficult to choose an optimal stopping criteria, as the validation function has multiple local minima (16 in the picture's case). It is left to the reader to investigate strategies to optimize early-stopping in these situations.

Furthermore, there are also scenarios in which, depending on the data presented, the validation loss is at first less than the training loss, as shown in Fig. 3.6.

In these situations, as a rule of thumb, we can use the following statements to determine the status of the training and decide when to stop.

- validation loss $>>$ training loss: over-fitting
- validation loss $>$ training loss: some over-fitting
- validation loss $<$ training loss: some under-fitting
- validation loss $<<$ training loss: under-fitting

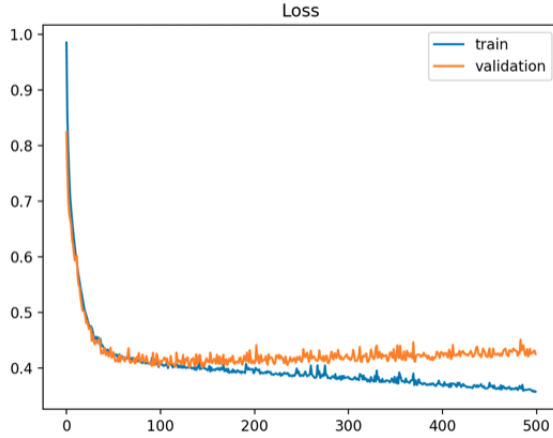


Fig. 3.6: Real-world example of the validation and training loss curve. The x axis is time, the y axis is the loss

3.8 Architecture

In the following sections we are going to briefly analyse the architectures of the models we are going to study to find characteristics and correlations.

For the sake of this paper, we are going to limit our analysis to some of the most common architectures for Convolutional Neural Networks which have been proven by other studies ([SIHvH18], [YKU⁺20], [Suh18]) to achieve promising results in the settings of sugar beet recognition. The architecture chosen are listed below and are treated in more detail in their respective sections.

- Alexnet
- VGG
- Resnet

3.8.1 Alexnet

Alexnet is a Convolutional Neural Network (CNN) architecture designed by Alex Krizhevsky in collaboration with Ilya Sutskever and Geoffrey Hinton. [KSH12]

The architecture is depicted in Fig. 3.7. The net is composed of eight layers: The first 5 are convolutional layers and the remaining three are fully-connected. The output of the last fully-connected layer is fed to a 1000-way Softmax which produces a distribution over the 1000 class labels. [KSH12]

As described by *Krizhevsky et al.* in [KSH12], the layers are defined as it follows:

- The first convolutional layer receive as input a $224 \times 224 \times 3$ image and filters it with 96 kernels of size $11 \times 11 \times 3$ with a stride of 4 pixels²
- The second convolutional layer takes as input the response-normalized and pooled output of the first layer and filters it with 256 kernels of size $5 \times 5 \times 48$.

²The stride is the distance between the receptive field centers of neighboring neurons in a kernel map

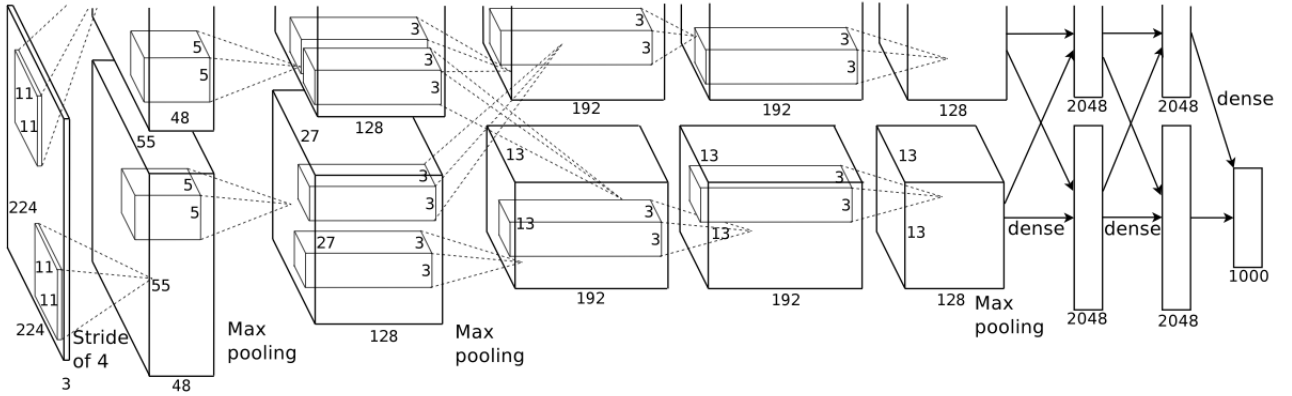


Fig. 3.7: Overview of the architecture of Alexnet [KSH12]

- The third layer has 384 kernels of size $3 \times 3 \times 256$ it is connected to the normalized and pooled output of the second
- The fourth convolutional layer has 384 kernels of size $3 \times 3 \times 192$ and it is connected to the third without pooling or normalization layers
- The fifth convolutional layer has 256 kernels of size $3 \times 3 \times 192$ and as input it receives the output of the forth.
- The fully-connected layers are composed of 4096 neurons each

3.8.2 VGG Networks

VGG stands for Visual Geometry Group at Oxford University and has been developed by Simonyan and Zisserman in [SZ15] for the ILSVRC (Image Net Large Scale Visual Recognition Challenge) 2014 competition ([RDS⁺14]). The concept of VGG net is similar to Alexnet: as the net increases, the number of convolutions and future maps increases as well. Rather than using 11×11 feature detectors or filters, however, the authors decided to use smaller 3×3 filters. The various architectures proposed in [SZ15] are shown in Fig. 3.8. In this paper, we are going to consider only the networks D and E, i.e. with 16 and 19 weight layers respectively. For the rest of the paper, we are going to refer to them as VGG16 and VGG19 respectively.

3.8.3 Residual Neural Networks (Resnet)

Many studies ([SZ15], [SLJ⁺14]) reveal that the depth of the Neural Networks is crucial and for most visual recognition tasks the trend has been to stack more layers into neural networks and increase their depth. ([SZ15], [IS15], [GDDM14], [HZRS14])

Training deeper networks like VGG19 and VGG16 (section n.3.8.2), however, is not a trivial task, since, once they start converging, the accuracy starts to saturate and then degrades quickly. This phenomena is due to the gradient vanishing during back-propagation, i.e. when the weights are updated, as it becomes smaller the more layers it goes through and vanishes before reaching the initial layer, hence they can not be updated.

ConvNet Configuration					
A	A-LRN	B	C	D	E
11 weight layers	11 weight layers	13 weight layers	16 weight layers	16 weight layers	19 weight layers
input (224 × 224 RGB image)					
conv3-64	conv3-64 LRN	conv3-64 conv3-64	conv3-64 conv3-64	conv3-64 conv3-64	conv3-64 conv3-64
maxpool					
conv3-128	conv3-128	conv3-128 conv3-128	conv3-128 conv3-128	conv3-128 conv3-128	conv3-128 conv3-128
maxpool					
conv3-256 conv3-256	conv3-256 conv3-256	conv3-256 conv3-256	conv3-256 conv3-256 conv1-256	conv3-256 conv3-256 conv3-256	conv3-256 conv3-256 conv3-256 conv3-256
maxpool					
conv3-512 conv3-512	conv3-512 conv3-512	conv3-512 conv3-512	conv3-512 conv3-512 conv1-512	conv3-512 conv3-512 conv3-512	conv3-512 conv3-512 conv3-512 conv3-512
maxpool					
FC-4096					
FC-4096					
FC-1000					
soft-max					

Fig. 3.8: Overview of the various architectures for VGG [SZ15]

He et al. in [HZRS15] tackled the problem of degradation with the introduction of a *deep residual learning* framework. At the core of the framework there is the so-called "residual block", shown in Fig. 3.9.

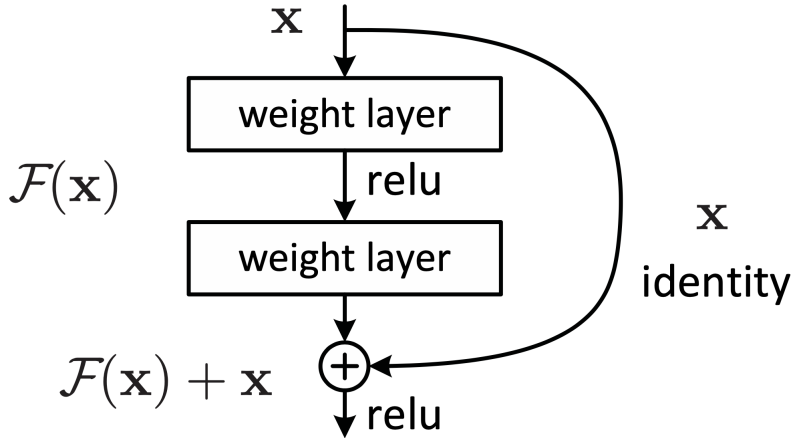


Fig. 3.9: Residual learning: a building block. [HZRS15]

Differently from plain convolutional networks, these blocks also have the so-called "identity connection" between the input and the output layer. In plain convolutional networks, the

layer name	output size	18-layer	34-layer	50-layer	101-layer	152-layer
conv1	112×112			7×7, 64, stride 2		
				3×3 max pool, stride 2		
conv2_x	56×56	$\left[\begin{array}{l} 3 \times 3, 64 \\ 3 \times 3, 64 \end{array} \right] \times 2$	$\left[\begin{array}{l} 3 \times 3, 64 \\ 3 \times 3, 64 \end{array} \right] \times 3$	$\left[\begin{array}{l} 1 \times 1, 64 \\ 3 \times 3, 64 \\ 1 \times 1, 256 \end{array} \right] \times 3$	$\left[\begin{array}{l} 1 \times 1, 64 \\ 3 \times 3, 64 \\ 1 \times 1, 256 \end{array} \right] \times 3$	$\left[\begin{array}{l} 1 \times 1, 64 \\ 3 \times 3, 64 \\ 1 \times 1, 256 \end{array} \right] \times 3$
conv3_x	28×28	$\left[\begin{array}{l} 3 \times 3, 128 \\ 3 \times 3, 128 \end{array} \right] \times 2$	$\left[\begin{array}{l} 3 \times 3, 128 \\ 3 \times 3, 128 \end{array} \right] \times 4$	$\left[\begin{array}{l} 1 \times 1, 128 \\ 3 \times 3, 128 \\ 1 \times 1, 512 \end{array} \right] \times 4$	$\left[\begin{array}{l} 1 \times 1, 128 \\ 3 \times 3, 128 \\ 1 \times 1, 512 \end{array} \right] \times 4$	$\left[\begin{array}{l} 1 \times 1, 128 \\ 3 \times 3, 128 \\ 1 \times 1, 512 \end{array} \right] \times 8$
conv4_x	14×14	$\left[\begin{array}{l} 3 \times 3, 256 \\ 3 \times 3, 256 \end{array} \right] \times 2$	$\left[\begin{array}{l} 3 \times 3, 256 \\ 3 \times 3, 256 \end{array} \right] \times 6$	$\left[\begin{array}{l} 1 \times 1, 256 \\ 3 \times 3, 256 \\ 1 \times 1, 1024 \end{array} \right] \times 6$	$\left[\begin{array}{l} 1 \times 1, 256 \\ 3 \times 3, 256 \\ 1 \times 1, 1024 \end{array} \right] \times 23$	$\left[\begin{array}{l} 1 \times 1, 256 \\ 3 \times 3, 256 \\ 1 \times 1, 1024 \end{array} \right] \times 36$
conv5_x	7×7	$\left[\begin{array}{l} 3 \times 3, 512 \\ 3 \times 3, 512 \end{array} \right] \times 2$	$\left[\begin{array}{l} 3 \times 3, 512 \\ 3 \times 3, 512 \end{array} \right] \times 3$	$\left[\begin{array}{l} 1 \times 1, 512 \\ 3 \times 3, 512 \\ 1 \times 1, 2048 \end{array} \right] \times 3$	$\left[\begin{array}{l} 1 \times 1, 512 \\ 3 \times 3, 512 \\ 1 \times 1, 2048 \end{array} \right] \times 3$	$\left[\begin{array}{l} 1 \times 1, 512 \\ 3 \times 3, 512 \\ 1 \times 1, 2048 \end{array} \right] \times 3$
	1×1			average pool, 1000-d fc, softmax		
FLOPs		1.8×10^9	3.6×10^9	3.8×10^9	7.6×10^9	11.3×10^9

Fig. 3.10: Overview of the Resnet architecture. The building blocks are shown in brackets [HZRS15]

output $\mathcal{H}(x)$ is obtained by:

$$\mathcal{H}(x) = \mathcal{F}(wx + b)$$

or

$$\mathcal{H}(x) = \mathcal{F}(x)$$

with w being the weights and b being the bias.

With the introduction of residual blocks, the output function assumes the form shown in equation n. 3.13, with x being the input.

$$\mathcal{H}(x) = \mathcal{F}(x) + x \quad (3.13)$$

Reworking the equation lets us obtain the so-called *residual function*:

$$\mathcal{F}(x) = \mathcal{H}(x) - x \quad (3.14)$$

The purpose of residual networks becomes to approximate the residual function, hence the difference between the input and the output. In other words, the aim is to learn the residual function in a way such that it approaches zero, hence making the identity value optimal.

The problem of the vanishing gradient is resolved by the identity function. During back-propagation the gradient can take this path and, since no weights are encountered, there won't be any change in the value computed by the gradient. This effectively allows the gradient to entirely skip the block and reach the initial layers and correct their weights. The architecture of residual networks we are going to use in this paper is shown in Fig. 3.10. For the rest of the paper, we are going to refer to them as "Resnet" followed by the amount of layers. For example, Resnet18 refers to the residual network having the 18 layers described in Fig. 3.10.

4 Analysing the Models

In this chapter, we will study how to properly perform tests on NNs to measure and analyse their characteristics and to find links among them in the context of the recognition of sugar beets. Although it is possible to predict some of the characteristics using NNs' weights ([UKG⁺20]), in this paper we will rely upon methods to find them empirically. The output of our investigation will be a toolbox which we can easily run on most devices to measure the characteristics we are mostly interested in.

In section 4.1 we will explore the concept of benchmarking in general terms to make an idea of the requirements we will need to full-fill to produce reliable results. In section 4.2 we will dive deep into measuring NNs' performances and we will introduce techniques we can use for our own benchmark. Finally, in section 4.3 we will describe the benchmark to use it in future sections to measure the characteristics of some networks.

4.1 Benchmarking

Benchmarking is a widely used tool to evaluate the performance of a system, either software or hardware, whose main goal is to produce consistent and precise measurements of said systems. High precision and reliability in benchmarks, however, have been always tricky to achieve and the complexity of these tasks have reached a high complexity in recent years, due to advanced processor designs and very intricate interaction between programs and operating systems. [BC18]

In addition, knowledge about the timing behaviour of tasks, more specifically their worst-case execution times (WCETs), is of the highest importance for building reliable and dependable real-time systems.[WDESP17]

According to *von Kistowski et al.* in [vKAH⁺15], benchmarks should follow certain key characteristics in order to be reliable:

- Relevance
- Reproducibility
- Fairness
- Verifiability
- Usability

4.1.1 Key Characteristics for a Correct Benchmark

4.1.1.1 Relevance

Relevance is probably the most important criteria for benchmarks. Relevance measures how close the behavior of the benchmark relates to the behaviors it is trying to test. [vKAH⁺¹⁵]

Even if the benchmark is realized perfectly and respects all the other characteristics, if the results do not provide relevant information they are of no use. It is when the relevance of the benchmark is taken into account that the computer scientists or engineers need to make the first trade-offs and the first considerations. As a matter of fact, benchmarks that are designed to be highly relevant in a specific scenario tend to have a narrow applicability; vice-versa, benchmarks with a broader spectrum are usually less indicative in specific scenarios. [vKAH⁺¹⁵]

Relevance also relates to the scalability of the benchmark. For example, benchmarks designed to test the full ability of servers might use the full resources that the server offers, for e.g. multi-threading, and as such it will not perform correctly in systems that do not have this possibility. [vKAH⁺¹⁵]

4.1.1.2 Reproducibility

Reproducibility is the ability to consistently obtain similar, if not equivalent, results if the benchmark is tested on the same environment. [vKAH⁺¹⁵]

Reproducibility is tightly correlated to the ability of describing the environment in perfect detail, so that it could be performed on the same environment and expect similar results. The hardware must be described perfectly and software versions must be included and documented, as well as every other configuration done on the system. Especially with the increase of complexity in modern hardware architecture and modern operating systems, variability in performance is introduced by several factors, including timing of thread scheduling, physical disk layout and user interaction. [vKAH⁺¹⁵]

Such variability can be addressed by running the benchmark for long enough periods of time in steady state, therefore without factors like user interaction.

4.1.1.3 Fairness

In order to create a perfect benchmark, fairness is a characteristic that should be taken into account. A fair benchmark is a benchmark that allows the results obtained in different systems with completely different hardware and software to be comparable. Benchmarks are simplistic and, by their very nature, include a certain degree of artificiality, so it is necessary to put some constraints in order to stop the programs to "exploit" them. Those restrictions can be put, for example, in the software used.

Kistowski et al. in [vKAH⁺¹⁵] pointed out, for example, a benchmark realized in Java requires a virtual machine on top of the operating systems and the choice of virtual machine can heavily influence the results. This shows how limiting software and hardware components must be carefully limited to ensure fairness in the results. However, putting too many limitations may actually hide some of the results, which might be relevant ([vKAH⁺¹⁵]). Therefore it is essential to find a good balance amongst the different limitations. Furthermore, portability plays a huge role in a fair benchmark. If too many

limitations are imposed, or if those limitations are too strict, a big pool of devices could be not suitable to run the benchmark. Similarly to the amount of limitations, portability is also a factor which requires a trade off. As a matter of fact, the portability of a benchmark strictly depends on the very nature of the devices which are set to be used.

4.1.1.4 Verifiability

A good benchmark should be able to provide trustworthy results and also results whose trustworthiness can be verified. To ensure the verifiability of the results, good benchmarks usually run some self-verification tasks during run-time, for e.g. if hyper-threading is still active when it should not. Moreover, it is also the case that some benchmarks let users configure some parameters. Those configurations should be documented, as an undocumented alteration might define the result as not trustworthy. [vKAH⁺¹⁵] Finally, it is also good practice to include more metrics in the results other than the ones strictly needed, since some red flags might be raised by inconsistencies in these metrics.

4.1.1.5 Usability

Usability is the characteristics of a benchmark which aims to remove roadblocks for users to run the benchmark in their environments. This feature is not limited to how easy it is to run the benchmark, which should be not a complex task, but some of the aforementioned characteristics relate to this one. For example, a good description of the benchmark also improves the usability of it, since it is easier to replicate. In addition, if the benchmark is too complex or expensive for its purpose it might limit a potential user and not allow them to effectively reproduce the tests.

4.1.2 Benchmark Techniques and Methodologies

This section will delineate the different methodologies used to measure the execution time of programs. It will contain techniques for both the *wall time* and the *CPU time*.

We are going to use the term *CPU time* to define the time spent by the CPU to process a piece of software, meanwhile we are going to use the term *Wall Time* to indicate the time elapsed between the start and the end of the execution of a program.

Measuring the wall time of a program is the most straightforward, as it can also be done analogically using a manual stopwatch: simply start the timer when the program starts and stop it when the program finishes. This method is undoubtedly imprecise and not very flexible, and it can only be applied in areas where the needed measurements are just rough approximation.[Ste01]

The equivalent method in UNIX-like systems is using the command *date*, which returns the system date and time. Due to the imprecise nature of such a method, it will not be described further.

An additional method, along the lines of the one described above, is using functions like *clock()* within the program we are trying to benchmark. This function needs to be used within the code of the program, similarly to the snippet of code n.4.1 [Ste01], therefore it is limited to measuring only small parts of the program.

In addition, such functions present two other problems. Since the function does not have

```

1 #include <time.h>
2
3 // ...
4
5 clock_t start, finish;
6 double total;
7 start = clock();
8 // Insert function here
9 finish = clock();
10 total = (double) (finish - start) / (double) CLK_TCK
11 printf("Total = %f\n", total);

```

Fig. 4.1: This snippet of code shows an example of use of the function `clock()`

a standardized implementation, the result may vary from device to device, which makes reproducibility impossible. Furthermore, this type of functions needs to be executed as well, similarly to any other function in the code, hence they might introduce overhead and noise in the measurements.

A better way to measure the *wall time* of a program is to use the UNIX command `time`. The synopsis for this program is the following ([Ker10]):

```
$ time [options] command [arguments ...]
```

Fig. 4.2: Synopsis of the command `time`

The `time` command runs the specified **command**, which runs a specific program, and, once the program has finished, it returns time-related statistics about the program's execution. These statistic consist of (*i*) the elapsed real time between start and end of the program, hence the wall time, defined as **real**; (*ii*) the CPU time, excluding I/O blocking functions, time for preemption and the time used for other OS related functions, defined as **user**, or user time; (*iii*) and the time spent by the OS to execute tasks on behalf of the user, defined as **sys**, or system time. The final one includes time for preemption and I/O blocking functions, or any other function associated with the program. [Ste01] It is worth noting that some shells have a built-in `time` command, hence may vary from the original one. To access the intended one, it is suggested to specify its path-name (for i.g. `/usr/bin/time`). [Ker10]

Nevertheless, we can run a small C++ program to give an example of how to use this command and to analyze its output. The snippet of the code can be seen in Fig.4.3. The program we are going to use simply accumulates numbers from 0 to 10000000000 and prints the result on screen. Before we start accumulating, however, we add a small delay, namely 1 second, to check if this will be counted in the CPU time. Once the code has been compiled, we can run it as shown in Fig.4.2, by writing "`time ./accumulate`" in the shell¹. From the result we can observe the three indications of time we described earlier (user,

¹"`accumulate`" is the name of the program and we assume to be in the correct directory

system and total time). In the case of the machine used for this paper, the user time was roughly 24,11 seconds, the system time roughly 0,05 seconds and the total time 25,254 seconds.

From these measurements, we can clearly observe that the total time is around one second bigger than the user time and the system time combined and it is due to the delay we introduced in line 6. If we comment out this line and we run the test once again, the total time now roughly equalizes the combination of user and system time (23,46s user 0,03s system, 23,578 total).

```

1 #include <iostream>
2 #include <chrono>
3 #include <thread>
4
5 int main(){
6     std::this_thread::sleep_for(std::chrono::milliseconds(1000));
7     double accumulate = 0 ;
8     for(double i= 0; i< 10000000000; i++)
9         accumulate += i ;
10    std::cout << "Result : " << accumulate << std::endl ;
11    return 0;
12 }
```

Fig. 4.3: Program used to test the command *time*

Even though the *time* command offers varied information, the time calculated and shown might not be fully reliable. As pointed out by *Beyer et al.* in [BLW17], this command does not reliably include the CPU time of child processes. This is due to the fact that the Linux kernel is able to count the CPU time of a child process, if that process terminated before the parent and the parent waited for it. In that instance, the CPU time of the child is lost and this will interfere with the precision of the measurements.[BLW17],

Beyer et al. in [BLW17] introduces yet another tool for benchmarks in their solution: control groups (cgroups). The Linux manual defines cgroups as "*a Linux kernel feature which allows processes to be organized into hierarchical groups, whose usage of various types of resources can then be limited and monitored*". [Ker21] Cgroups therefore allow the user to assign processes to a group and every child process spawned by the assigned process will be tracked down.

Cgroups were initially released with Linux 2.6.24, however, due to the problems with the initial version, starting from Linux 3.10, cgroups version2 has been introduced. In this paper, we will not describe the differences between the two versions, as it is not the purpose of this paper (we refer to the Linux manual for further details²) and the *controllers* we are interested in did not change in functionality. *Controllers* allow the user to easily control and measure a specific resource within each group. [BLW17]

The following *controllers* are the ones we are most interested in:

cpu can guarantee a minimum number of CPU resources, even when the system is busy. However, this does not limit a CPUs usage if a free CPU is present

²<https://man7.org/linux/man-pages/man7/cgroups.7.html>

cpuacct provides information about the accumulated CPU usage

cpuset restricts the number of CPU cores available to a cgroup. Additionally, in a system with more than one CPU and nonuniform memory access (NUMA), it restricts the process to a subset of the physical memory [BLW17]

freezer enables suspending and resuming of all processes in the group

pids enables the limiting of the number of spawnable processes.

In addition to a more precise calculation of the CPU time, *cgroups* also augment the fairness and the verifiability of the benchmark. By limiting the resources of a more powerful machine, the benchmark can have similar results to a much less powerful one, hence increasing fairness. Although this approach may hinder usability, as it is more cumbersome to set up than using the *time* command, the benefits in precision make up for this trade-off.

4.1.3 Common Practices in Benchmarking

In section 4.1.2, we already discussed some of the issues which can be encountered when trying to design benchmarks. The pitfalls, however, are not limited to those challenges; on the contrary, it is notoriously difficult to obtain consistent results when designing benchmarks. In this section, we will explore some techniques to effectively reduce the non-determinism of lots of features, both hardware and software, which intend to increase performances. In most cases, since we have little to no control over them, the solution will be to disable those features. Although it will effectively get rid of the non-determinism, the environment we are going to create does not reflect how the application will run on a real application, however it would allow us to obtain consistent results.

The first element we are going to analyse is Turbo-boost. This feature will automatically make the processor core run faster than the marked frequency. *Acun et al.* in [AMK16] calculated an execution time difference of up to 16% amongst processors on the Turbo Boost-enabled supercomputers. Since we have little control over it, the only solution to limit this variation is to completely disable it. The commands to permanently disable it are shown in Fig. 4.4.

```
# Intel
2 echo 1 > /sys/devices/system/cpu/intel_pstate/no_turbo
# AMD
4 echo 0 > /sys/devices/system/cpu/cpufreq/boost
```

Fig. 4.4: Command to disable turbo boost in both AMD and Intel devices

Modern CPUs often employ a technique called Simultaneous multi-threading (SMT) to speed up execution. This technique makes it possible for two threads to run simultaneously on the same core sharing execution resources, like the cache or ALU. In the case of Intel processors, the implementation of this technology is called Hyper-threading.

As a result of this implementation, it might occur that the sibling thread steals cache space, for example, from the workload we want to measure. To avoid these situations and

limit the number of CPU-migrations, we will need to disable Hyper-threading by turning down the sibling thread in each core as shown in Fig. 4.5.

```
# X being the CPU number
2 echo 0 > /sys/devices/system/cpu/cpuX/online
# To check the pair of CPU x
4 /sys/devices/system/cpu/cpuX/topology/thread_siblings_list
```

Fig. 4.5: Command to disable Hyper-Threading

Another technique we can use to reduce noise in our measurements is to bind a process to a certain CPU core. In Linux we can do that with the *taskset* tool. [Ker21]

Furthermore, we can increase the process priority with the command *nice*. Processes with higher priority will get more CPU time since the Linux scheduler will favour them, compared to processes with normal priority of 10. [Ker21]

A further step to take is to set the scaling governor policy to be *performance*. The scaling governor changes the clock speed of the CPUs on the fly to save battery power, because the lower the clock speed, the less power the CPU consumes. To set the policy to be *performance* one can use the method described in Fig. 4.6.

```
for i in /sys/devices/system/cpu/cpu*/cpufreq/scaling_governor
2 do
    echo performance > $i
4 done
```

Fig. 4.6: Command to set the scaling governor policy to be *performance* for every CPU

4.2 Benchmarking Deep Neural Networks

Now that we have understood benchmarks and the characteristics they should possess, we can explore in greater depth how we can benchmark Deep Neural Network (DNN).

As expressed by Reddi *et al.* in [RCK⁺20], "Designing ML benchmarks is different from designing traditional non-ML benchmarks". As a matter of fact, the spectrum of tasks NNs can perform is very broad. Consequently there is a wide spectrum of requirements they need to fulfil, making the development of a reliable and relevant benchmark, which would simultaneously be universal, impracticable. Additionally, in this paper, we are interested in measuring performances in image classification tasks in the context of sugar beet recognition. And although benchmarks are usually designed to compare performances, the scope of our investigation is to precisely measure the characteristics of Neural Networks and to find possible correlations amongst them.

4.2.1 Benchmark Inference Time

As we have already delineated in section n.3.3, inference time is one essential characteristic of DNN and in some cases fast inference time is an important requirement, therefore

speeding up calculations is of vital importance. To achieve faster inference time, and faster calculations in general, DNNs are trained and run on GPUs, which, in turn, means exploiting their hardware acceleration capabilities and their asynchronous execution (multi-threading). ([CCG17], [GDP09], [CBB17], [PJY⁺13], [OJ04])

In order to measure inference time, we can apply the watchdog approach we discussed earlier in section 4.1.2 as shown in Fig. 4.7. As we already stated in the previous section, multi-threading is a factor which must be taken into account when performing benchmarking, since it could be a source of indeterminism. To prevent that, in the snippet of code in Fig.4.7, taken from the benchmark developed by *Bianco et al.* in [BCCN18], there is a call to the function *torch.cuda.synchronize()*. This function is used to synchronise the host and the device, i.e. GPU and CPU, so the time is recorded only after the processes running on the GPU are terminated. Whilst overcoming arguably one of the biggest issues, further inspection of the code reveals some potential errors.

```

1 def measure(model, x):
2     # synchronize gpu time and measure fp
3     torch.cuda.synchronize()
4     t0 = time.time()
5     with torch.no_grad():
6         y_pred = model(x)
7     torch.cuda.synchronize()
8     elapsed_fp = time.time() - t0
9
10    return elapsed_fp

```

Fig. 4.7: Imprecise way to benchmark for inference time [BCCN18]

Although the function *time.time()* is insinuated to be better and more accurate than the UNIX equivalent in the python documentation³, it calculates the CPU time and would not be accurate if the model is run on a GPU. One way to prevent this is to use a CUDA event. Pytorch provides a useful wrapper class for them, namely *torch.cuda.Event*⁴. Moreover, GPU initialization must be taken into account as well. When the GPU is not used, it enters a lower power state in which the GPU shuts parts of the hardware down. In this state, any program which invokes the GPU will cause the drive to load anew, or the GPU to initialise once again, processes which might need a significant amount of time. It is therefore necessary to run the model multiple times - before measuring inference time. [Gei21] Finally, one must be careful with transferring data between the CPU and GPU. This is usually done accidentally, when the tensor is created on the CPU and then run on the GPU. This memory allocation process takes a considerable amount of time, which will have an impact on the measurements. [Gei21] With these corrections, a more precise measurement for inference can be found with the snippet of code in Fig. 4.8.

For the purpose of this paper, we are, purposely, going to mainly explore techniques which can be applied to Unix-like operating systems. However, there are techniques which can

³<https://docs.python.org/3/library/time.html#time.time>

⁴<https://pytorch.org/docs/stable/generated/torch.cuda.Event.html>

```

1 def measure(model, x):
2     device = torch.device("cuda")
3     model.to(device)
4     dummy_input = torch.randn(1, 3, 224, 224, dtype=torch.float).to(device)
5     start = torch.cuda.Event(enable_timing=True)
6     end = torch.cuda.Event(enable_timing=True)
7     timings=np.zeros((repetitions,1))
8     #GPU WARM UP
9     for _ in range(10):
10        _ = model(dummy_input)
11    # MEASURE PERFORMANCE
12    with torch.no_grad():
13        for rep in range(300):
14            start.record()
15            _ = model(dummy_input)
16            end.record()
17            torch.cuda.synchronize()
18            timings[rep] = start.elapsed_time(end)
19    mean_syn = np.sum(timings) / repetitions
20    std_syn = np.std(timings)
21    print(mean_syn)

```

Fig. 4.8: More precise way to measure inference time

be applied to other types of devices, as well. For example, in case the models need to be run on a mobile device, Tensorflow Lite provides benchmarking tools to measure inference time, both in warming up and steady state. [AAB⁺15a]

For Android devices, the benchmark can be run with the command shown in Fig. 4.9.

```

1 adb shell am start -S \
2   -n org.tensorflow.lite.benchmark/.BenchmarkModelActivity \
3   --es args '"--graph=/data/local/tmp/your_model.tflite' \
4   '--num_threads=4'

```

Fig. 4.9: Method to benchmark on Android with Tensorflow Lite [AAB⁺15a]

The result of this command is a log file which can be accessed by the command shown in Fig.4.10.

```
adb logcat | grep "Average inference"
```

Fig. 4.10: Command to access the measured inference time in Tensorflow-Lite [AAB⁺15a]

Finally, since this paper is mainly focused on detecting sugar beet plants from images, and since Convolutional Neural Networks (CNNs) became dominant for image recognition tasks ([YNDT18]), it is also worth mentioning that inference time for this class of Neural Networks can be calculated manually, knowing the architecture of the model. Inference time is the time the model needs to forward propagate an image through each layer, i.e.

it is the amount of computations needed to be performed at each of the steps. These operations are defined as Floating Point Operation, or FLOP. The amount of FLOPs is different for each layer and requires different information to be computed.

In case of the convolutions layers, the number of FLOPs is calculated with the following equation:

$$C_FLOPs = 2 \times Nk \times Ks \times Os \quad (4.1)$$

where:

Nk - number of kernels

Ks - kernel shape (3x3, 5x5, 7x7, etc.)

Os - Output shape

For the fully connected layers, the amount of FLOPs is defined as:

$$FCL_FLOPs = 2 \times Is \times OS \quad (4.2)$$

where:

Is - Output shape

Os - Output shape

For the pooling layer, the number of FLOPs also depends on whether there is a stride, or not. In case of a stride-less pooling layer, the formula to use is the following:

$$PL_FLOPs = H \times D \times W \quad (4.3)$$

where:

H - height of the image

D - depth of the image

W - width of the image

In case of a stride, equation n.4.3 becomes:

$$PL_FLOPs = (H/S) \times D \times (W/S) \quad (4.4)$$

where:

S - stride

To better understand the use of the aforementioned equations, we can calculate the FLOPs of the neural network described in Fig.4.11.

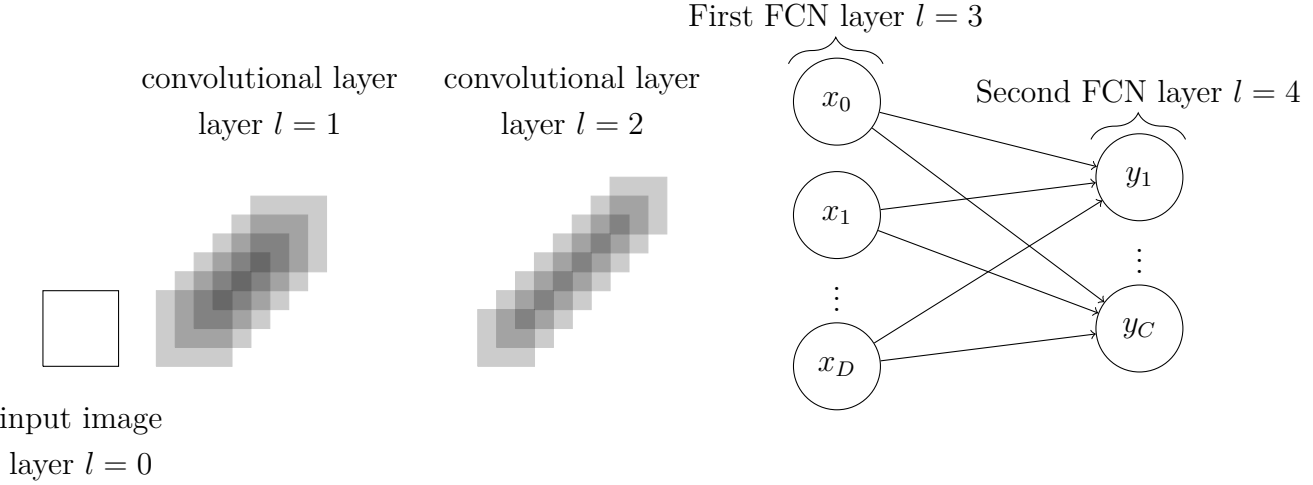


Fig. 4.11: Architecture of the convolutional neural network used as an example to calculate inference time. Layer $l = 0$ is the input layer, with dimension $28 \times 28 \times 1$; $l = 1$ is the first convolution layer with a kernel of $3 \times 3 \times 5$ and an output shape of $26 \times 26 \times 5$; $l = 2$ is the second convolution layer with a kernel of $3 \times 3 \times 5$ and an output shape of $24 \times 24 \times 5$; $l = 3$ is the first fully connected layer (FCN) with an input size of $24 \times 24 \times 5$ and an output size of 128; $l = 4$ is the second FCN, and final layer, with an input size of 128 and an output size of 10

The total number of FLOPs is given by:

$$\begin{aligned}
 & \text{FirstConvolution} - 2x5x(3x3)x26x26 = 60,840 \text{ FLOPs} \\
 & \text{SecondConvolution} - 2x5x(3x3x5)x24x24 = 259,200 \text{ FLOPs} \\
 & \text{FirstFCLayer} - 2x(24x24x5)x128 = 737,280 \text{ FLOPs} \\
 & \text{SecondFCLayer} - 2x128x10 = 2,560 \text{ FLOPs} \\
 & \text{FLOPs} = 60,840 + 259,200 + 737,280 + 2,560 = 1,060,400
 \end{aligned} \tag{4.5}$$

Supposing that the processor used performs at 1 Giga FLOPS (Floating Point Operations per Second), the inference time is given by:

$$\begin{aligned}
 \text{InferenceTime} &= \frac{\text{FLOPs}}{\text{FLOPS}} \\
 &= \frac{1,060,400}{1,000,000,000} \\
 &= 0.0010604 \\
 &= 1,0604ms
 \end{aligned} \tag{4.6}$$

Equation n.4.6, however, only reveals a theoretical and ideal value for inference time. As a matter of fact, even though the number of FLOPs remains constant, the amount of FLOPs in a processor might not. The number of FLOPs is calculated as :,

$$\text{FLOPS} = \text{Number_of_Cores} \times \text{Average_frequency} \times \text{Operations_per_cycle} \tag{4.7}$$

Although the number of cores is an easy-to-find and stable value, the average frequency

and operations per cycle are not. The operating frequency is usually a lower bound of the actual operating frequency, and in modern processors may vary drastically due to technologies such as TurboBoost(Intel) or Turbo Core(AMD). For example, a modern Intel®Core™ i7-4500U Processor has a base frequency of 1.80 GHz, but it can reach 3.00 Ghz with TurboBoost.⁵. To have an estimation of the FLOPs of your machine, we can use the Intel MKL benchmark suite, which solves linear systems of equations to estimate them. [ZS21].

4.2.2 Benchmark Training Time

As we discussed already in section n 3.2, the training time is the time needed by the model to update its weights. Learning is usually done in *epoch*, which defines one cycle through the full training dataset ([AR20]). The number of epochs is defined by the modeller and it can drastically influence the time needed for training. Logically, since more epoch means more cycles, hence more calculations, more time would be needed to complete the training. Some libraries already provide tools which measure training time, like for example *fast.ai*. When the wrapper function *fit_one_cycle()* of the class *Lerner* is invoked (at the end of every epoch) it returns - in addition to the metrics defined by the user (like accuracy, or error rate) - the time required for that epoch. An example can be seen in table 4.1. Such results can also be saved in a csv file at the end of the process.

epoch	train loss	valid loss	accuracy	time
0	2.310583	0.764163	0.767841	28:27
1	1.031493	0.420149	0.874435	30:12
2	0.549505	0.350187	0.889792	31:15
3	0.369313	0.336940	0.891599	30:15

Table 4.1: Metrics obtained from the *fast.ai fit_one_cycle()* function. The time is in minutes

However, if higher precision or control is needed, training time can also be calculated using the watchdog approach, as shown in Fig. 4.12. Even though a bit of overhead is introduced with more function calls, this overhead usually does not impact the measurement significantly. Furthermore, if the training is done on a GPU, we can refer to a similar discussion to the one we made in section 4.2.1. In the example in Fig. 4.12 is used, however CUDA events should be used for even higher precision, similarly to Fig.4.8.

4.2.3 Measuring Accuracy

As mentioned in section n. 3.4, accuracy is, perhaps, one of the most looked-after metrics in a neural network. During the analysis of training time, we are going to use the accuracy provided for us by *Fastai* at each epoch. *fastai* calculates the accuracy during validation by calculating the mean between two tensors, as shown in Fig. 4.13. [fas21]

⁵Intel Documentation

```

1   time_elapsed = []
2   for epoch in range(1, args.epochs + 1):
3       # start time
4       torch.cuda.synchronize()
5       since = int(round(time.time() * 1000))
6       train(args, model, device, train_loader, optimizer, epoch)
7       torch.cuda.synchronize()
8       time_elapsed[epoch] = int(round(time.time() * 1000)) - since
9       print ('training time elapsed {}ms'.format(time_elapsed[epoch]))
10      print ('training time elapsed ' + str(sum(time_elapsed)) + 'ms')

```

Fig. 4.12: Benchmark for training time using the watchdog approach

```

1 def accuracy(inp, targ, axis=-1):
2     "Compute accuracy with `targ` when `pred` is bs * n_classes"
3     pred, targ = flatten_check(inp.argmax(dim=axis), targ)
4     return (pred == targ).float().mean()

```

Fig. 4.13: Function in fast.ai that calculates the accuracy [fas21]

4.3 Benchmarking Tool for Neural Networks

Following the characteristics delineated in section n. 4.1.1 and the techniques we analysed in sections n. 4.1.2 and n. 4.2, we can build a tool which allows us to study the behaviour of Neural Networks.

Conceptually, the behaviour of the test is shown in Fig. 4.14.

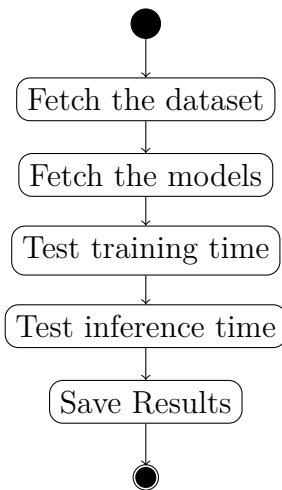


Fig. 4.14: Behaviour of the benchmarking suite on a conceptual level

The tool will allow us to study the behaviour of neural networks in order to find correlations amongst the metrics we analysed in chapter n. 3, therefore the main requirement it needs to adhere to is flexibility. Applications in the field of sugar beet recognition may be subject to various requirements and different conditions, hence the tool must be able to reflect that. In other words, it should be flexible enough so that we are able to configure it in multiple ways to reflect the various condition, but at the same time it must also be able to

produce results that are specific for our scope, i.e. finding the correlation between different metrics. Furthermore, we need the results to be verifiable and trustworthy. Being the foundation for further steps, the results need to be trustworthy and they need to be precise and accurate enough, so that they can be reasoned about.

Finally, we are expecting the tool to be run on multiple devices, hence usability is also a factor to pay attention to. If the tool is too difficult to set up or run, it will lead to mismanagement of time and resources.

Flexibility is also a key factor for the choice of the dataset. Studies in the field of weed recognition use various techniques to collect the images for their datasets. For example, authors of [LY20] use the BOSCH's Bonirob system, a field robot, to collect various data about the plants, while authors of [BHC18] use Unmanned Aerial Vehicles (UAVs). Moreover, the way images are labelled is dataset dependent. Therefore, in order to ensure flexibility, the user must have full control over the dataset and how it is represented in the tool.

As already discussed in section n. 3.8, the choice of the architecture is limited amongst Resnet, Alexnet and VGG. The models which can be analysed will be the ones listed below.

- Resnet18
- Resnet34
- Resnet50
- Resnet101
- Resnet152
- Alexnet
- VGG16
- VGG19

Both the indication regarding the dataset and the choice of the models will be indicated in an external configuration file by the user. The tool will read this file before initializing the test, in order to collect the necessary information needed to run properly. This configuration file helps to improve both flexibility and usability, in addition to automatically creating a documentation of the run for reproducibility.

To further increase usability, a logging system is implemented so that information about the run and potential errors are visible to the user and can be corrected.

The actual implementation of the tool is done using Python and revolves around the *fastai* library. This library is built on top of Pytorch, a very common library for machine learning, and offers powerful functions and high flexibility without a significant drop in performance. [HG20]

Fastai perfectly suits the goals of the benchmarking tool as it is "*approachable and rapidly productive, while also being deeply hackable and configurable*". [HG20]

Thanks to *fastai*, we also have the possibility to use publicly available implementations of the models listed above, thus removing possible differences in results coming from divergent implementations.

In the following sections, we are going to describe how the training process and the inference time are analysed.

4.3.1 Analysing the Training Process

epoch	time	accuracy
0	00:16	15.25710374116897
1	00:16	35.62246263027191
2	00:15	44.72259879112243
3	00:16	48.03788959980011
4	00:16	50.67659020423889
5	00:16	51.96211338043213
6	00:15	54.22868728637695
7	00:16	54.769957065582275

Table 4.2: Example of training time results

Training time is the primary characteristic of a model which can reveal some important information and can be used to optimise applications. Fastai provides 3 functions for training a model, namely *fit()*, *fit_one_cycle()*, and *fine_tune()*, and each of these functions has a different purpose.

The function *fit()* is simply a wrapper around the *train()* function of PyTorch and it represents a very basic training loop.[fas21]

On the other hand, *fit_one_cycle()* implies a phenomenon called *Super-Convergence* which allows fast training of Neural Networks exploiting the learning rate. [ST17] One of the key elements of super-convergence is training with the one-cycle policy developed by *Smith* in [Smi18]. [ST17]

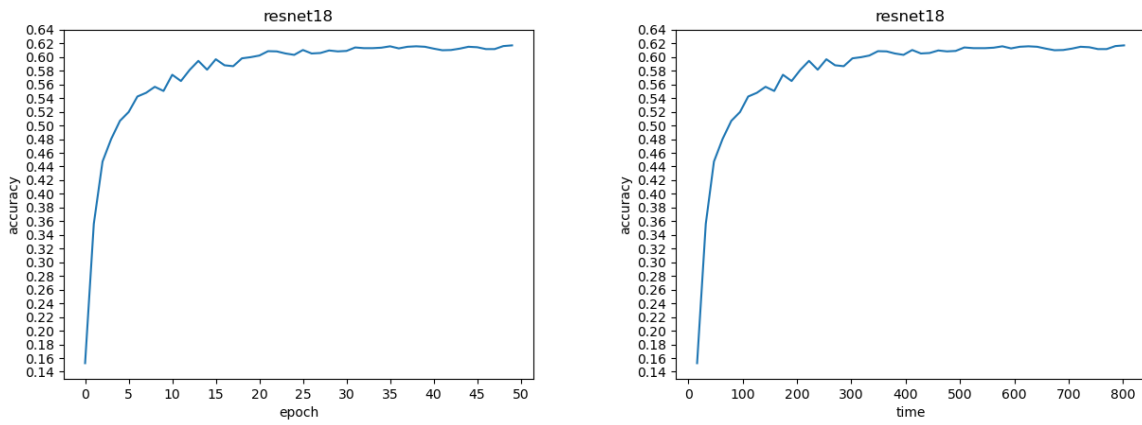
Finally, *fine_tune()* can be seen as a particular combination of *fit_one_cycle()* and *(un)freeze* which works well in a variety of cases. *fine_tune()* is geared mainly towards transfer learning, i.e. towards training pre-trained models with a new dataset, since it employs the *freeze()* function. Such function is used to freeze the first layers so that the weights do not get updated during further training.[fas21]

Since the three functions have different scopes and are beneficial in different areas of applications, the benchmarking tool is configurable in a way that the preferred way of training can be chosen.

Once the models and the training method have been selected, the tool will start training each model according to the number of epochs chosen by the user. Once the training is complete, the results are stored and then represented into a graph.

As suggested in section n. 4.2.2, there are two ways to record training time. For the purpose of this paper, we will use the first one, i.e. the one offered by *fastai*. Even though the second method (Fig. 4.12) is more precise, it does not give actual indications about the time taken for each epoch. On the other hand, this method neglects the time taken to validate the training step, hence overlooking this small delay for every epoch. As a result the total training time does not comprise this delay which, even though potentially insignificant, it increases gradually as the number of epochs increase and it will influence

the total training time. However, using the first method, we also have information of the accuracy obtained at each epoch and thus allowing us to better reason about it. Table 4.2 shows an example of the information extracted from this process. Furthermore, this information is then extrapolated and graphed, as shown in Fig. 4.15a and Fig. 4.15b and saved as a serialised file.



- (a) Example of the accuracy graphed against the number of epoch used to train for resnet18 (b) Example of the accuracy graphed against time taken to train in seconds for resnet18

Fig. 4.15: Example of graphs produced by the tool when analysing training time

4.3.2 Analysing inference Time

As described in section n. 3.3 inference time is the time needed for the model to make predictions. We discussed in section n. 4.2.1 different ways to measure inference time, including how to calculate it, considering the architecture of the Neural Network we chose. This last method, however, is not suitable for our purpose, since it is not precise enough to lead to correct predictions, therefore the method used for the benchmark tool is the one shown in Fig. 4.8, with the only difference that the tool will save the prediction result and calculate the total accuracy achieved. The results will be then graphed as shown in Fig.4.16.

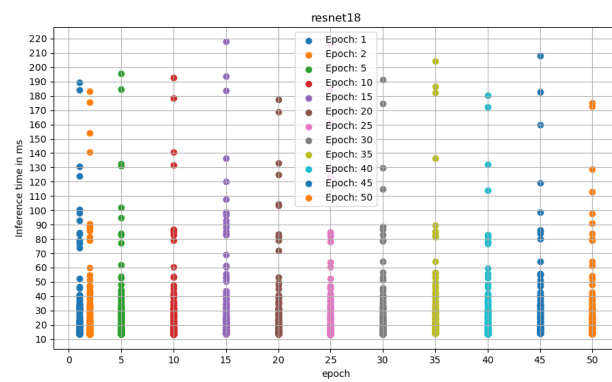


Fig. 4.16: Example of the graphs produced by the tool when analysing inference time

Fig. 4.16 shows an example of Resnet18 trained for various epochs and tested using 50

images which were not part of the training set. During the analysis of inference time, the tool will calculate accuracy as the percentage of corrected predictions over the whole set, as shown in equation n. 3.4. Since we are not going to treat any binary classification problem, we are going to avoid equation n. 3.5.

Inference time is analysed based on the number of epochs used for training the models. A complete overview of the process is shown in Fig. 4.17.

The user indicates a list containing all the epoch to use for training. For example, in Fig. 4.16 the epoch inserted were:

1, 2, 5, 10, 15, 20, 25, 30, 35, 40, 45, 50

Once the model has been trained for the respective number of epochs and the inference has been tested, the results are saved and the model initialised. The process ends when the inference time of all the models have been trained for each epoch in the list.

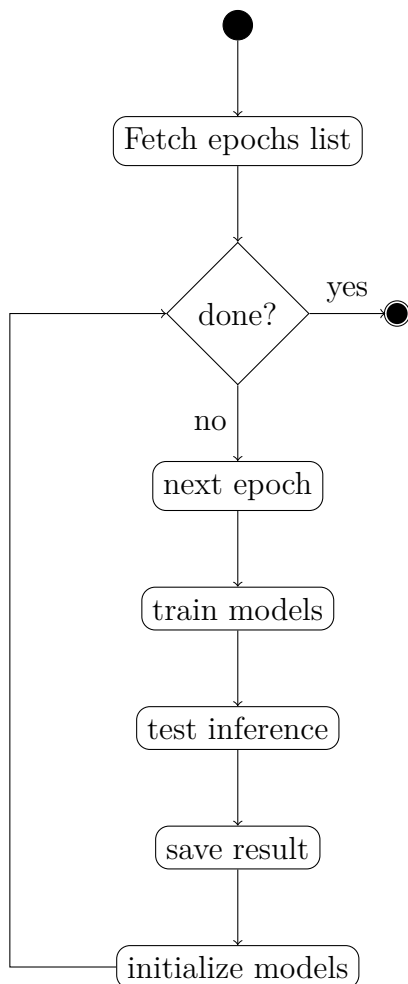


Fig. 4.17: Overview of the process to test inference

4.3.3 Further Analysis

Once the tests terminate, the tool stores the information collected in a file on the disk. The information stored are:

- Epoch
- Training loss
- Validation loss
- Accuracy
- Training time for epoch
- Inference Time
- Prediction
- Ground Truth

The data, however, is serialised before being saved, therefore it can be visualised and further investigated with the use of a ready-to-use Jupyter notebook ([KRKP⁺16]). In addition to the raw visualisation of the data, the notebook allows the user to elaborate information for further analysis. This notebook calculates the average training time needed for each epoch, the highest accuracy achieved during training and the highest accuracy during the prediction test. Furthermore, it also calculates precision (equation n. 3.7), recall (equation n. 3.8) and the F1-score (equation n. 3.12).

The notebook also gives the possibility to graph the trend of the single models during the test, over both training time and epochs. In addition to the trend, during training - as discussed in section n. 4.3.1 - it is also possible to visualise the validation loss and training loss over training time.

5 Analysis of the characteristics

In this chapter, we will analyse and measure different characteristics from various Neural Network architectures with the purpose of finding useful correlations which we can use in a later stage. In order to achieve this goal, we will use our understanding from chapter 3 of each metric of Neural Network and the tool we developed in section 4.3.

In challenges such as the ImageNet classification challenge ([RDS⁺15]) the ultimate goal is to achieve the highest accuracy possible, neglecting other performance metrics like inference time. [CPC16]

Although accuracy is of high importance, in practical applications other metrics are to be considered as well, depending on the different requirements. As pointed out by *Canziani et al.* in [CPC16], metrics like inference time, parameters and operations count are hard constraints for the deployment of Neural Networks in practical applications. Furthermore, training time is often a time consuming process which highly depends on factors like the complexity of the task, size of the network and training set ([PE89]).

Finding relations between these metrics and other factors as well, like influence of a given input feature to the prediction of the model ([HEKK19]), will allow us to optimise applications, saving time and resources in the process.

5.1 Test Environment

All the experiments have been run on the same machine running Ubuntu 20.04.3 LTS (Focal Fossa). For the specific of the machine, please refer to table 5.1

CPU	2x AMD EPYC 7452 32-Core Processor
CPU MHz	1499.324
CPU max MHz	2350,0000
CPU min MHz	1500,0000
Total memory	1 TB (16x64 GB)
GPU	Nvidia A100-PCIE-40GB
Number of GPUs	7

Table 5.1: Specifics of the machine which run the experiments

It is assumed for all the use cases that, if no specification is made, the training of the models has been carried out by the *fit_one_cycle()* function present in fastai using the default learning rate. Furthermore, the models have not been pre-trained, hence no transferred learning is applied, and the models have been trained using full precision.

5.2 Fist Experiment

For this use case, we are going to use the dataset proposed by *Giselsson et al.* in [GJJ⁺17], which we are going to refer to as the ‘plant_seedlings_v2’ dataset. This dataset contains ~1000 RGB images with a resolution of 10 pixels per mm divided in 12 different plant species. The plants in the dataset are listed in table 5.2. This dataset contains pictures of one of the most common weeds found in sugar beet plantations, a plant commonly referred to as “charlock”. [CM10]

Even though the dataset is mainly focused on seedlings and it contains pictures of other plants as well, this will give us proper insights of the models’ behaviours in a farming setting.

English	Latin
Maize	Zea mays L.
Common wheat	Tricicum aestivum L.
Sugar beet	Beta vulgaris var. altissima
Scentless Mayweed	Matricaria perforata Mérat
Common Chickweed	Stellaria media
Shepherd’s Purse	Capsella bursa-pastoris
Cleavers	Galium aparine L.
Redshank	Polygonum persicaria L.
Charlock	Sinapis arvensis L.
Fat Hen	Chenopodium album L.
Small-flowered Cranesbill	Geranium pusillum
Field Pansy	Viola arvensis
Black-grass	Alopecurus myosuroides
Loose Silky-bent	Apera spica-venti

Table 5.2: Categories of the ‘plant_seedlings_v2’ dataset [GJJ⁺17]

The first metrics we are going to analyse are training time, number of epochs and accuracy. We will study those metrics in order to recognize some patterns and use those to be able to find correlations between the three, with the final aim being able to predict one of them, whilst knowing the others. These prediction patterns can be used to save time during the learning process in future applications, as we can estimate the accuracy before starting the process.

The tool ran the test three times for 50, 100 and 200 epochs. We are going to start our analysis by studying the results obtained when trained for 100 epochs, which are shown in Fig. 5.1 and 5.2.

Alexnet is the model that achieved the lowest accuracy, overall reaching ~86% after 99 epochs. The highest accuracy has been achieved by Resnet101, peaking at ~97% after 66 epochs. Moreover, VGG16 and VGG19 achieved the same peak accuracy at ~95%, however VGG16 required 13 epochs less (43 compared to the 56 needed for VGG19). Similarly, Resnet18 and Resnet34 achieved comparable top accuracies at 94.39% and 94.48% respectively, however Resnet34 required considerably less time to reach this

number peaking after 62 epochs, while Resnet18 achieved this number when the training cycle was almost done, namely after 96 epochs. An overview of the performances of all the models can be seen in table 5.3.

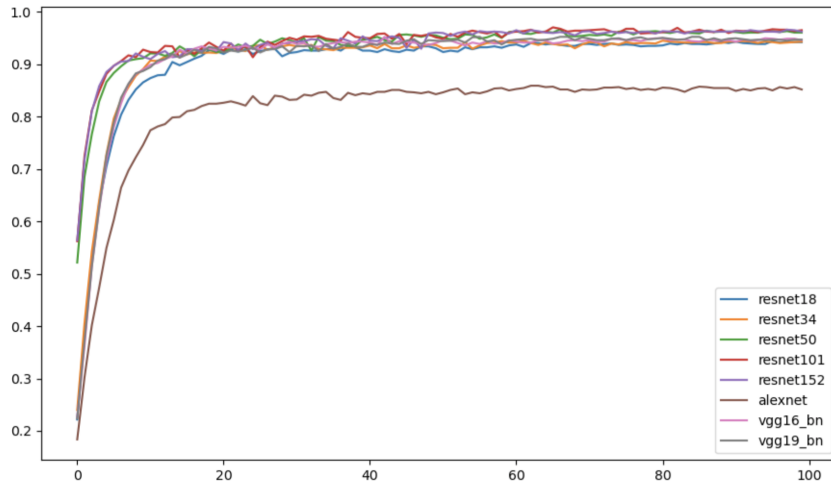


Fig. 5.1: Accuracy achieved by the models after being trained for 100 epochs. The x axis is the number of epochs, while the y axis is the accuracy achieved

Model	Top Accuracy (%)	Epochs needed	Average Time (s)	Total Time (s)
Resnet18	94.39	96	7	747
Resnet34	94.48	62	9	876
Resnet50	96.65	67	14	1439
Resnet101	97.01	66	21	2101
Resnet152	96.56	98	29	2851
Alexnet	85.88	63	7	705
VGG16	95.20	43	17	1743
VGG19	95.20	56	20	1952

Table 5.3: Performances of the models trained with the 'plant_seedlings_v2' dataset for 100 epochs

Fig. 5.1 shows the response of all models during the training based on the epoch used for training. The response of the model shows that, within the first ten epochs, the accuracy increases quickly and tends to stabilise afterwards, increasing slowly over time. However, we can observe a compact graph, meaning all the models (besides Alexnet) achieved accuracies not too far off from each other. As a matter of fact, the difference in accuracy between the highest performing model (Resnet101) and the lowest performing model (Resnet18) was only 3%.

Fig. 5.2, on the other hand, depicts the accuracy graphed over training time. Alexnet took the least amount of time to finish the training cycle (747 seconds), however Resnet18 took only ~40 seconds more and reached a far better accuracy(94% compared to 85%). Resnet152 took 47 Minutes and 30 Seconds (2851 seconds) to complete the test and is the

model that required the most time.

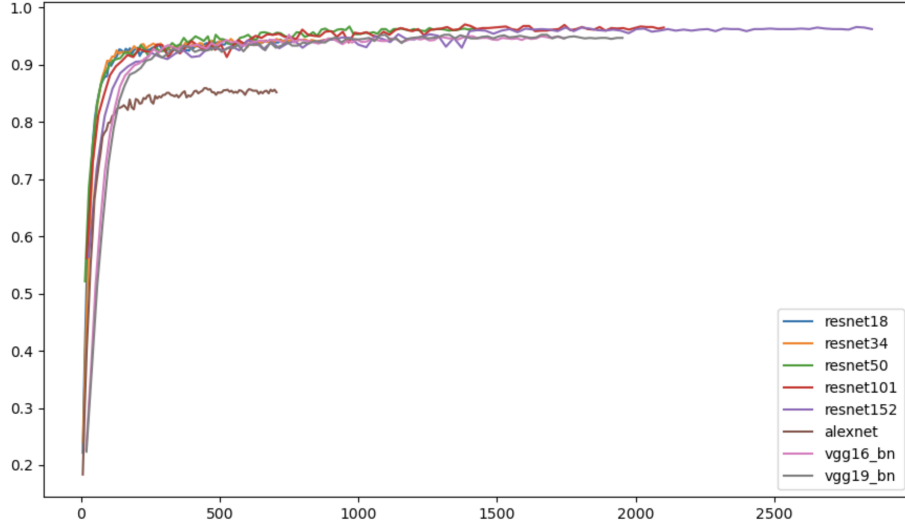
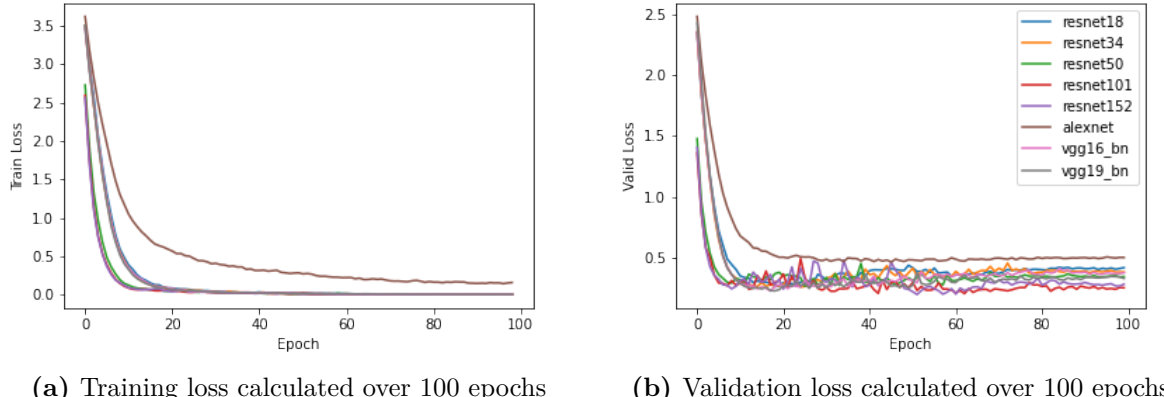


Fig. 5.2: Accuracy achieved when training for 100 epochs in relation with training time. The x axis is the training time in seconds, while the y axis is the accuracy achieved



(a) Training loss calculated over 100 epochs

(b) Validation loss calculated over 100 epochs

Fig. 5.3: Training loss and validation loss of all models calculated over 100 epochs

In Fig. 5.3, we can analyse the loss calculated for the models during the training. As shown in Fig. 5.3a, all the models (besides Alexnet) reached 0 loss within the first 30 epochs. This means that, theoretically, the models learned the dataset perfectly within the first 20 epochs. Usually, when the training loss is 0, we are expecting a case of over-fitting, which would be proven by a high validation loss. We can then study the validation loss of the models in Fig. 5.3b. From their response, we can observe that the validation loss does not increase drastically like we saw in the first experiment. On the contrary, we can see in table 5.4 that the difference between validation loss and training loss is rarely more than 0.4. Furthermore, the curve seems to be quite stable, especially for shallower networks, and the validation loss tends to increase slowly.

For example, we can analyse the trend for the model which reached the highest accuracy overall, namely Resnet101, shown in Fig. 5.4a. As shown in table 5.4, the difference at the

Model	Difference
Resnet18	0.42
Resnet34	0.38
Resnet50	0.35
Resnet101	0.25
Resnet152	0.28
Alexnet	0.34
VGG16	0.38
VGG19	0.33

Table 5.4: Difference between validation loss and train loss after 100 epochs

end of the training is 0.25. Moreover - as we suspected before - the training loss approaches zero within the first 30 epochs, while the validation loss remains stable for the entire training process, with some spikes at around the 30 epochs. Furthermore, the validation loss becomes higher than the training loss at around 10 epochs.

We can observe a similar behaviour in the response of Resnet152 (Fig. 5.4b). The training loss approaches zero once more around the 30 epochs and becomes smaller than the validation loss at around 10. Although the validation loss tends to stabilise for this model, as well, the graph shows a less stable behaviour with more fluctuations between 20 and 50 epochs.

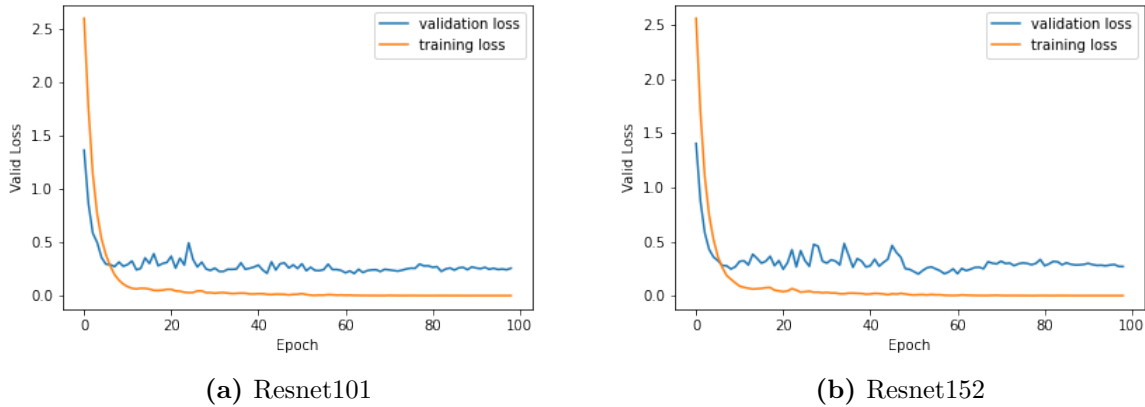


Fig. 5.4: Training loss and validation loss of Resnet101 and Resnet152 over 100 epochs

In addition to the training time, we can also use the benchmark tool we developed to measure and analyse the inference time of each model.

As we are mostly focused on sugar beet recognition, it is safe to assume use cases where field robots would scan the field to recognize the vegetation, similarly to the one proposed by *Lottes et al.* in [LHS⁺16b]. In such setting, the time taken to classify the image, ultimately, results in a soft deadline, as the time taken to scan the field is greatly influenced by it, therefore being able to estimate the needed inference time could help optimise this part of the application.

In order to test for inference time, we are going to use a dataset composed of ~120 pictures taken from the original dataset. These pictures were taken before starting the process, therefore they have not been used for training. The results are shown in Fig. 5.5.

Fig. 5.5a shows the inference time based on the accuracy, while figure 5.5b shows the inference time based on the epoch used to train.

From Fig. 5.5a we can start to observe some rather interesting properties. For each model, as they achieve accuracy less than 88%, the inference time is rarely measured to be more than 60 ms, with only 2 exceptions (~100ms and ~390ms). Furthermore, the only model that achieved an accuracy smaller than ~82% is Alexnet¹.

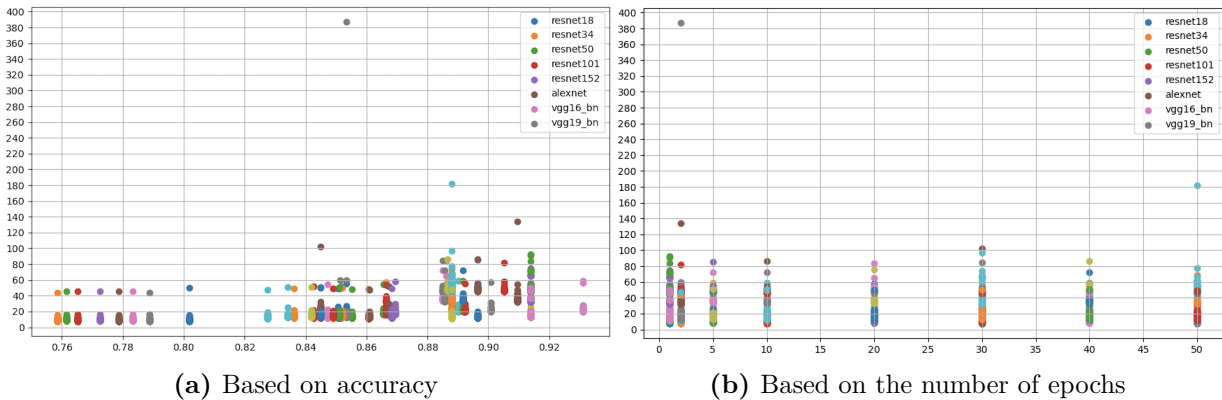


Fig. 5.5: Inference time measured for each model using the dataset discussed previously. The inference time is in milliseconds, while the accuracy for Fig. 5.18a is the percentage of correct predictions.

For accuracies over 88%, although the behaviour of the models seems to be less compact, the inference time rarely measures more than 100 milliseconds, with only two outliers (~135ms and ~180s).

From Fig. 5.5b we can see that, with the exception of the outliers we identified before, the number of epochs that measured the highest value for inference is 30. As a matter of fact, when trained for different numbers of epochs, the models never require more than 100 milliseconds to process the images.

A closer investigation of the individual performance of each model shows further interesting aspects. For the purpose of this experiment, we are going to analyse only Resnet101 and Resnet152, whose behaviour is shown in Fig. 5.6a and Fig. 5.6b respectively. For both models, we can see that the highest accuracy is achieved when trained for only one (~91% for both) and two epochs (slightly lower of 91% for Resnet18 and ~90% for Resnet152). For the other epoch, the accuracy achieved was consistently lower than 90%.

In the case of Resnet101, the fastest training time has been achieved when trained for ten and five epochs, with an inference time of over 45 milliseconds on only two occasions. Although the fastest, the model trained with these epochs also achieved the lowest accuracy. The slowest inference time has been achieved when the model has been trained for two epochs, with an inference as high as 135 milliseconds. However, the model achieved the worst performance when trained for 30 epochs. As a matter of fact, even though it measured the lowest inference time when trained for two epochs, this occurred in only

¹The whole results can be seen in Fig. A.5

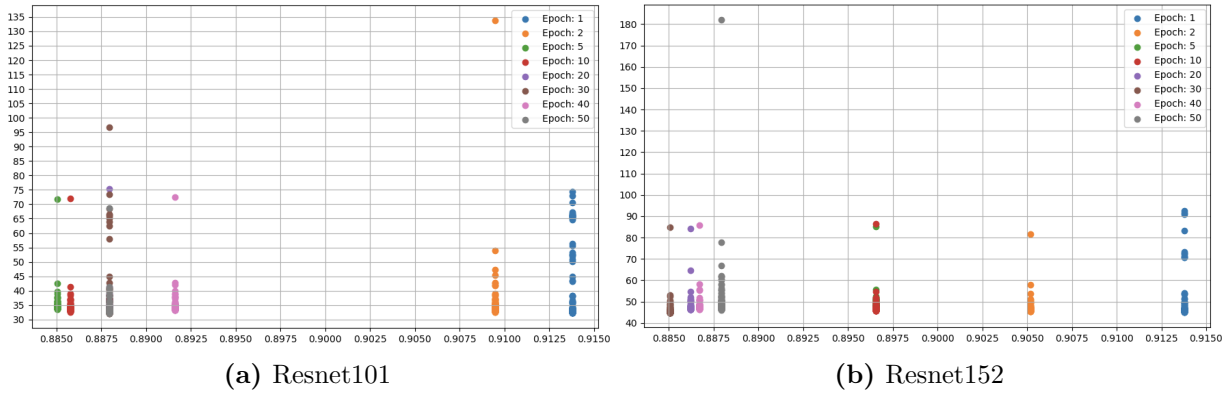


Fig. 5.6: Inference time measured for Resnet101 and Resnet152. The inference time is in milliseconds, while the accuracy is the percentage of correct predictions.

one case, while, when trained for 30 epochs, for a considerable amount of pictures, the inference time was in a range between 57 and 95 milliseconds.

Resnet152, on the other hand, showed more consistent results, with an inference time being in the range of 40 to 90 milliseconds for all epochs with the exception of one case where it reached 180 milliseconds. The fastest inference time for this model is measured when the model has been trained for 20 epochs.

From this investigation we can conclude that the performances of these two models are quite comparable, when it comes to inference. Both in terms of inference time and accuracy achieved, the two models show similar results, albeit for different levels of training.

For example, in the case of Resnet152, with a training time of 580 seconds (20 epochs), we obtain a model that can make predictions in a range between 45 and 85 milliseconds with an accuracy of ~89%. In the case of Resnet101, we can obtain similar results (prediction time between 70 and 30 milliseconds with an accuracy of ~89%) with a training time of 210 seconds (10 epochs).

We can also run the tool to discover which pictures took the most amount of time to be processed. Fig. 5.7 shows the ten slowest images for each model graphed based on their sizes.

The graph shows a rather compact and stable behaviour, with the slowest time measured for images having a size bigger than 1500 kb.

For pictures of more than 100 kb and less than 300 kb, the inference time is between 0 and 100 ms, with each model performing rather similarly.

For this experiment, both for training and for testing inference, we used a dataset with images having rather similar size and resolution, therefore this analysis is not as valuable as expected.

However, we can run the tool to make modifications on the images of the dataset. As a matter of fact, the tool also allows one to make a copy of the pictures in the dataset and transform them into grey-scale. Therefore, we can double the amount of pictures in the dataset by including grey-scale copies of those.

The results of the first run are shown in table 5.5. When compared to table 5.3, we can observe that all the models have reached better accuracy besides Alexnet. As a matter of fact, Alexnet peaked at ~80%, while all the other models peaked at accuracies over 95%. The best accuracy has been achieved by Resnet101 (~99%) in 80 epochs. Furthermore,

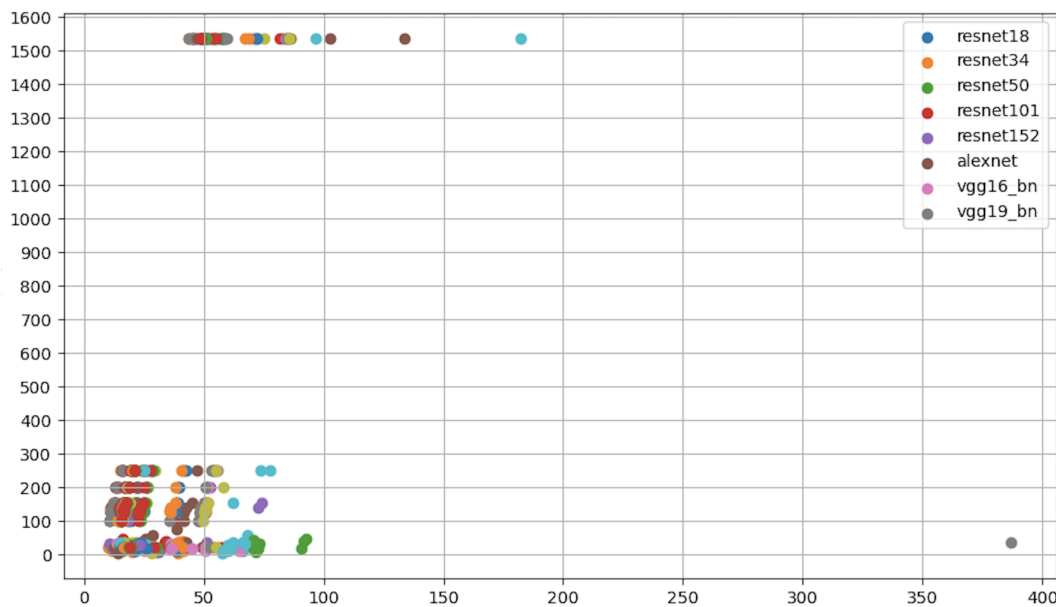


Fig. 5.7: This graph shows the size in kb (y axis) of the ten slowest images over the time taken to be processed (x axis)

this time around, in comparison to the previous run, all the models took more time to train, with a difference in average time for epoch being from one second (Alexnet) to 23 seconds (Resnet152). This is the result of introducing more pictures in the dataset, which makes the training process more time-consuming.

Model	Top Accuracy (%)	Epochs needed	Average Time (s)	Total Time (s)
Resnet18	95.98	82	9.16	916
Resnet34	96.72	90	12.67	1267
Resnet50	98.15	82	23.66	2366
Resnet101	99.12	80	37.05	3705
Resnet152	98.84	85	52.01	5201
Alexnet	79.81	89	8.12	812
VGG16	97.27	93	29.87	2987
VGG19	96.77	64	33.74	3374

Table 5.5: Performance of the models trained for 100 epochs on the 'plant_seedlings_v2' dataset including the grey-scale variant of the pictures

The analysis of the training loss and validation loss trends also offers quite different results. An overview can be seen in table 5.6. The difference in loss between the validation and the training set decreased quite substantially. For example, Resnet101 and Resnet152, which were also the ones with the lowest difference in the previous run (see table 5.6), measured a difference of only 0.07 and 0.08 respectively.

Fig. 5.8 shows the trend for the two models. We can observe that the training loss

approaches zero after around 30 epochs, while the validation loss tends to decrease further and stabilises after around 80. It is also worth pointing out that, in the case of Resnet101, the validation loss starts to increase after around 10 epochs and, since the training loss is already approaching zero, it would satisfy the criteria for an early stopping of the training. However, right after the 20 epochs mark, the validation loss decreases once again, up until it becomes only slightly larger than the training and then stabilises afterwards.

Model	Difference
Resnet18	0.20
Resnet34	0.18
Resnet50	0.12
Resnet101	0.07
Resnet152	0.08
Alexnet	0.20
VGG16	0.12
VGG19	0.14

Table 5.6: Difference between validation loss and train loss after 100 epochs using the gray-scale variants of the pictures

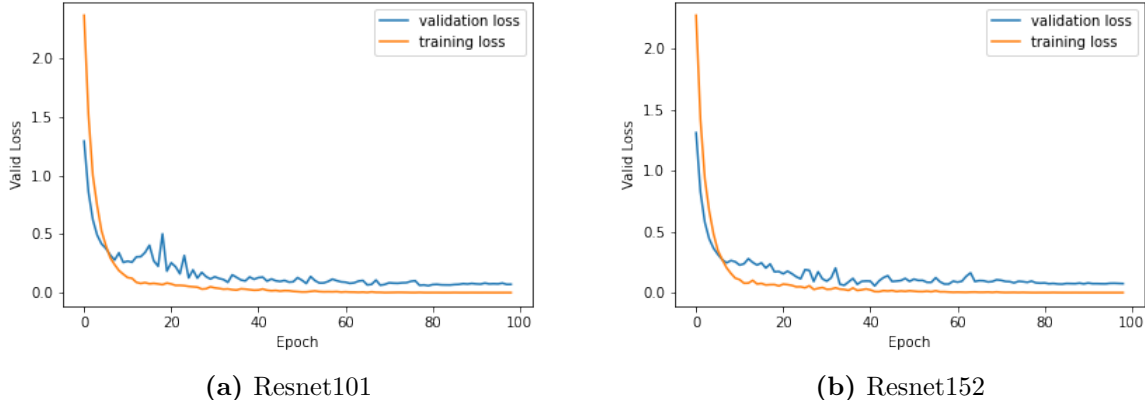


Fig. 5.8: Training loss and validation loss of Resnet101 and Resnet152 over 100 epochs on the 'plant_seedlings_v2' dataset and the grey-scale variant of the pictures

From the information acquired so far, we would expect the models to perform better during the inference time test. Fig. 5.9 shows the results of the tests. In Fig. 5.9a, the performance of the models has been tested using the same inference dataset we used for the results in Fig. 5.5a. Comparing the two graphs, we can observe that the accuracy dropped significantly. As a matter of fact, without the grey images for training, the lowest accuracy achieved was around ~75%, while in this run we calculated accuracies at around ~69%. Furthermore, the highest accuracy calculated in this run is around ~88%, while in the run before the highest achieved was ~92%. The inference time did not improve as well, as the models showed a comparable or even worst response time for the images at each epoch. Interestingly, when we observe the overall trend of the models, we can see that as the accuracy increases, it appears that they require more time to process the images and

make their predictions.²

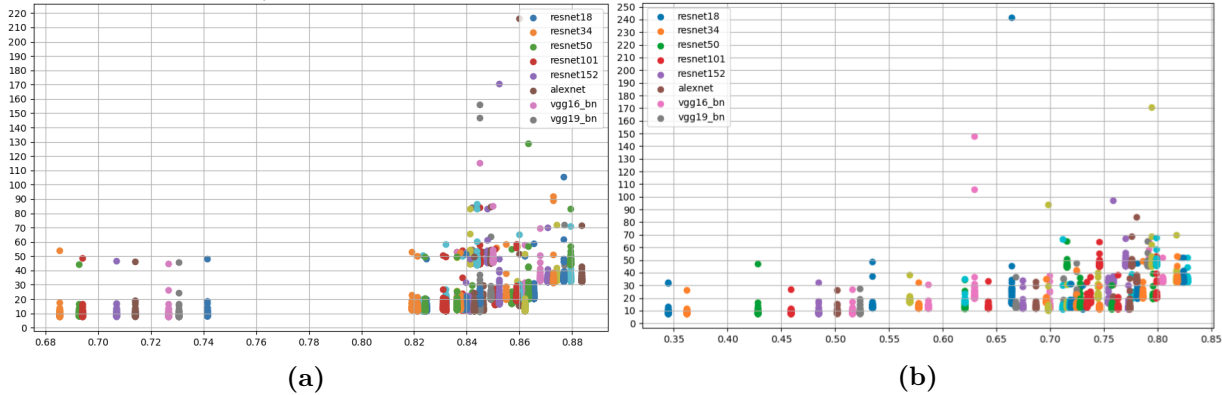


Fig. 5.9: Inference time of each model trained with grey images as well. In Fig. 5.9a, the inference is calculated using the same dataset used in Fig. 5.5a, while in Fig. 5.9b the dataset is composed with the same pictures, but in grey scale.

From Fig. 5.9b, on the other hand, we can see the inference time of the models using the same image we used before, but in grey-scale. In this run, the accuracy dropped to a lowest point of ~35%, a considerable downgrade from the ~75% of the original run. The highest accuracy, on the other hand, dropped to ~85%, i.e. similar to the ~88% of before. In this run, the overall inference time failed to improve, as well, but rather tended to increase as the accuracy increases.³

From these analyses we can conclude that, for this dataset and for these models, including grey-scale versions of the images increases the performances in training, but negatively effects the inference performances of the models.

5.3 Second Experiment

In this experiment, we are going to use the dataset proposed by *Vevaldi et al.* in [PVZJ12], which will be referred to as "the Pets dataset" for the remainder of this paper. This dataset is directly accessible from the library and contains 37 categories of pets, with roughly 200 pictures each.

Even though this dataset contains pictures that are not necessarily related to agriculture, we can use it to obtain information about the behaviour of the models when confronted with images that have different characteristics than the ones we expect. For example, in a farming environment, it is safe to assume that each picture will have similar backgrounds, while this dataset has images with backgrounds that differentiate quite heavily with one another. We can use this dataset, therefore, to compare the results with our first use case, hoping to obtain more useful information.

The first metrics we are going to analyse are the number of epochs, training time and accuracy.

²The whole results can be seen in Fig. A.6

³The whole results can be seen in Fig. A.7

The benchmarking tool ran the test for each model using three different amounts of epochs, i.e. different training time, in order to simulate three different scenarios: one example with low length of training time, one with a medium length of training time and finally one with a very high length of training time. The tool ran with ten, fifty and a hundred epochs, respectively.

The one scenario which yielded more promising results and the one we are going to analyse first is the one with fifty epochs. Fig. 5.10 shows the results of each model's accuracy graphed against the number of epochs used for training, while Fig. 5.11 shows the results of each model's accuracy graphed against the necessary training time needed to reach that accuracy.

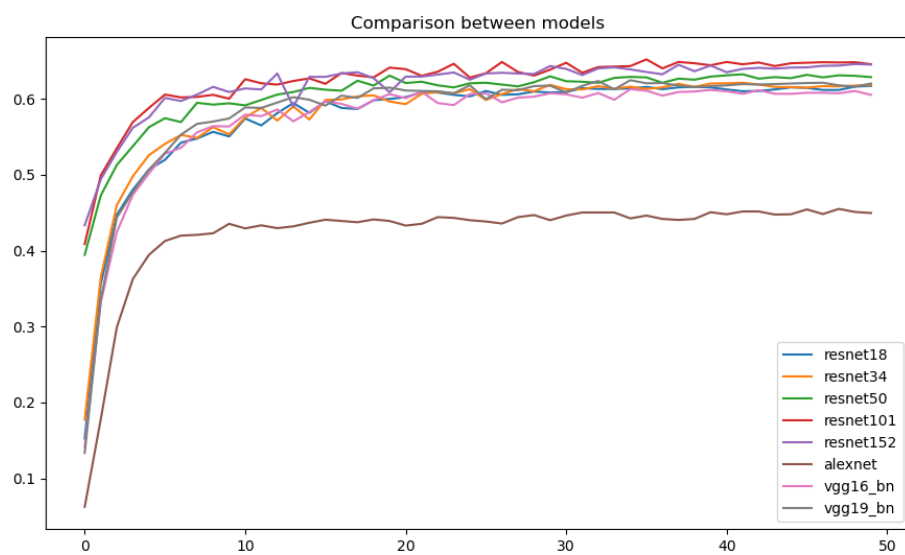


Fig. 5.10: Accuracy achieved by the models over 50 epochs. The x axis is the number of epoch, while the y axis is the accuracy achieved

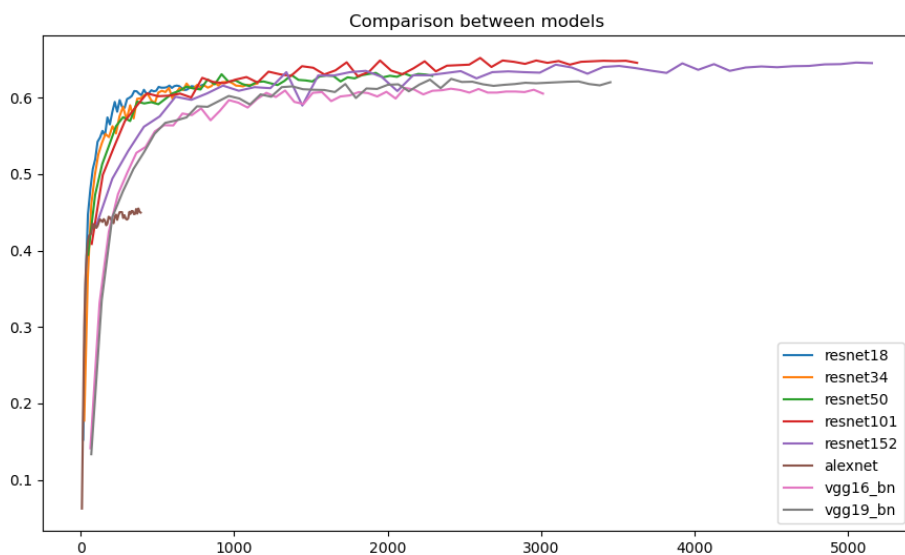


Fig. 5.11: Accuracy achieved by the models during the training phase plot over training time. The x axis is the training time in seconds, while the y axis is the accuracy achieved

As suspected, for each model, the accuracy grows logarithmically higher as the number of epochs increments, or as the training time increments. A closer inspection of Fig. 5.11 lets us derive other conclusions. Alexnet finishes training in considerably less time compared to the other networks (~6 minutes), albeit reaching the lowest accuracy overall (45%). We can observe this difference in time by looking at Fig.5.12 and Fig.5.13, which shows the behaviour of Alexnet, Resnet101, Resnet152 and VGG19 in the same settings.

As also shown in the previous graphs, Resnet101 achieved the best overall accuracy at around 65% with a training time of ~62 minutes, followed by Resnet152, which needed ~90 minutes to reach an accuracy of ~64%. Finally, VGG19 took ~60 minutes to reach an accuracy of 61%.

In order to collect more information about the response of the model, we should take a closer look at how they performed individually.

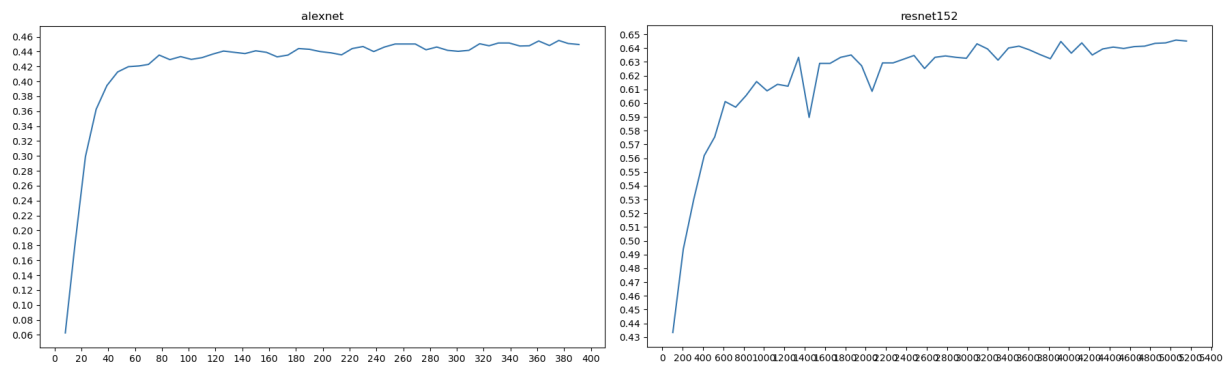


Fig. 5.12: Accuracy of Alexnet and Resnet152 against training time in seconds

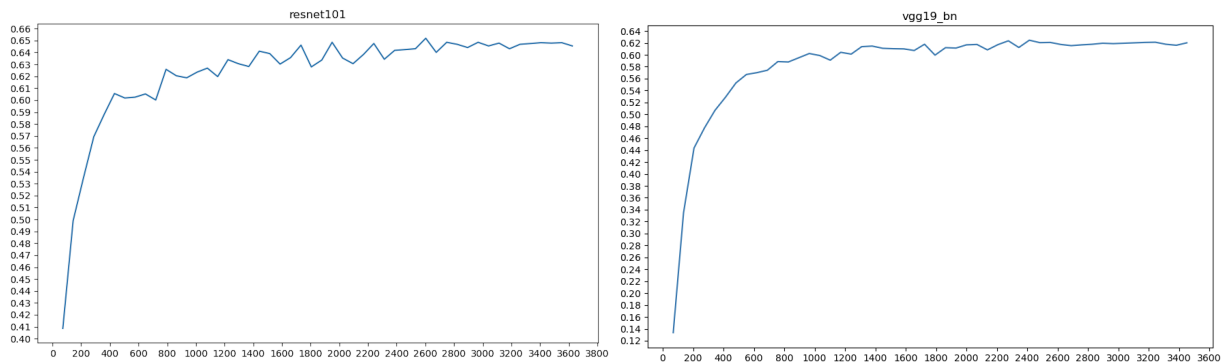


Fig. 5.13: Accuracy of Resnet101 and VGG9 against training time in seconds

Fig.5.12 and Fig.5.13 also show how stable each model was during training. The stability we are observing, in this instance, is how fluctuating each model has been during training, regarding its accuracy. The less fluctuating it is, the better we able to predict the accuracy from the training time, or the number of epochs, and vice-versa. From the results, we can see that Resnet152 and Resnet101 tend to fluctuate more compared to Alexnet or VGG19 (Fig. 5.13).

Such fluctuation, however, does not hide a trend which is common amongst all models:

after a certain number of epochs, the accuracy tends to stabilise and grow significantly slower. Fig. 5.10 can help us locate the point at which the accuracy stops increasing at a high rate at around 10 epochs and this is further proved by Fig. 5.14.

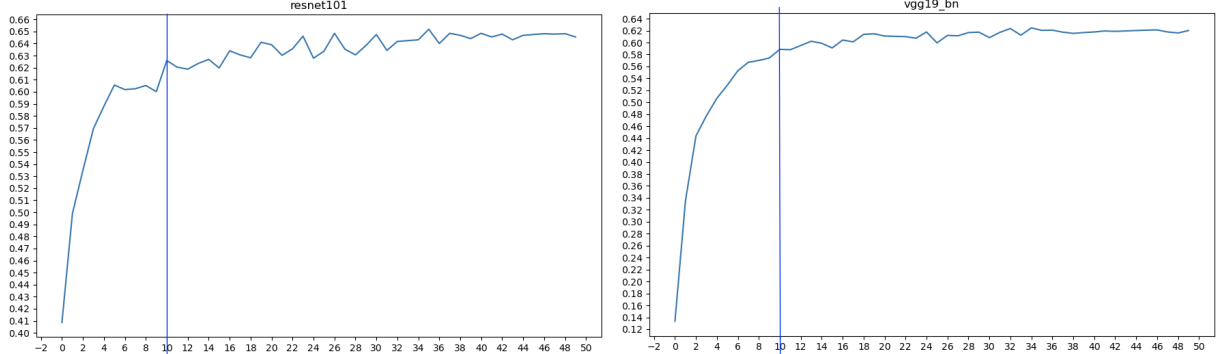


Fig. 5.14: Breaking point of Resnet101 and VGG19

We can further analyse the behaviour of each model for the first 10 epochs by observing Fig. 5.15. This graph gives us a closer look at how the models have been trained and how the curve looks like. Differently from the previous graph, Resnet152 this time reached a higher accuracy, however it was also the model that took the most time to fully complete the training.

On the other hand, from Fig. 5.15, we can clearly observe that, if compared with each other for the same training time, shallower networks like Resnet34 or Resnet50 achieved higher accuracy than deeper networks like Resnet152. This is obviously due to the fact that, within the same training time, shallower networks manage to complete more epochs, and therefore complete more training cycles. As a matter of fact, if we were to compare models on an epoch base we will find that deeper networks will achieve better accuracy when given the same number of epochs.

If we observe Fig. 5.11 before the 1000 seconds mark, we can see that Resnet18's curve starts to flatten, reaching an accuracy of ~61%, while the others tend to reach smaller accuracy values. Around the 1000 seconds mark the behaviour of all the models starts to equalise and afterwards the accuracy of deeper networks will increase reaching higher values. As mentioned previously, this is due to the models being able to finish more epochs within the same time frame. In this case, the models reached to finish the training completely, as shown in 5.11. Models from different architectures do not follow this trend. Alexnet, as we already discussed above, does not manage to reach somewhat close to the same accuracy of the other models. VGG16 and VGG19 follow similar trends and both curves overlap multiple times. Even though VGG19 is considerably bigger than VGG16 ([SZ15]), they reach very similar accuracy even before the 1000 seconds marks with very similar training time.

This behaviour is further highlighted in Fig. 5.16 which shows the behaviour of the models trained for 100 epochs. We can see that once again around 1000 seconds the curve of every model starts to flatten and the models using the Resnet architectures achieve similar

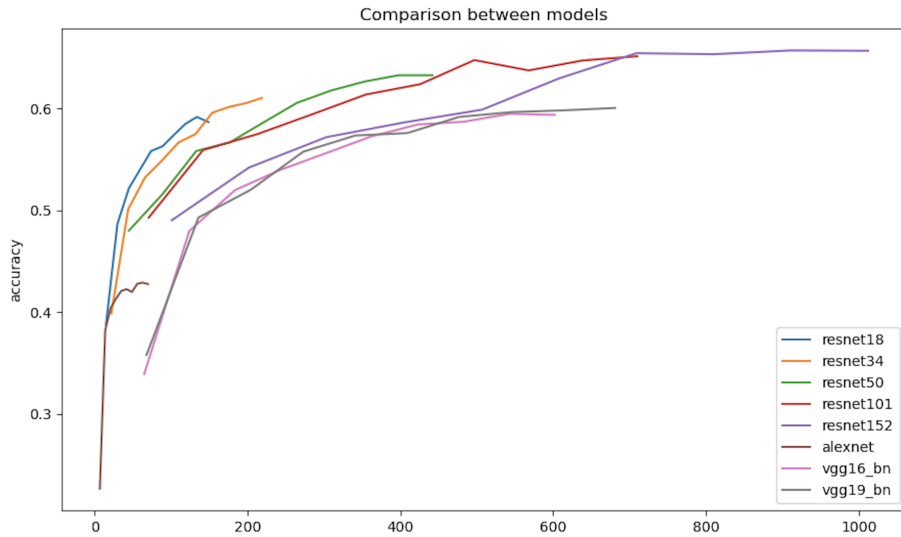


Fig. 5.15: Accuracy achieved by the models over 10 epochs. The x axis is the training time in seconds, while the y axis is the accuracy achieved

accuracy. The highest accuracy is achieved by Resnet152, which also needed the most training time. Surprisingly, Resnet50 performed better than Resnet101, achieving better accuracy with less training time. VGG16 and VGG19 performed similarly, displaying overlapping curves, with VGG19 once again requiring more training time.

More importantly, however, this graph confirms the results and the hypothesis we made previously. Furthermore, we can use all the data we acquired to calculate the average training time required for each epoch. The results are provided in table 5.7.

Model	Time (s)
Resnet18	15.01
Resnet34	22.0
Resnet50	45.02
Resnet101	72.11
Resnet152	102.02
Alexnet	7.01
VGG16	60.09
VGG19	68.97

Table 5.7: Average time for each epoch

Comparing the training results we just obtained with the ones obtained for the 'plant_seedlings_v2' dataset, we can see that, regardless of the raw values we obtained, the models behaved equivalently in training.

Training for 100 epochs also gives us more complete insights regarding the future performance of our models. In other words, we can determine when the model starts to over-fit or under-fit and when to stop the training to avoid future poor performances.

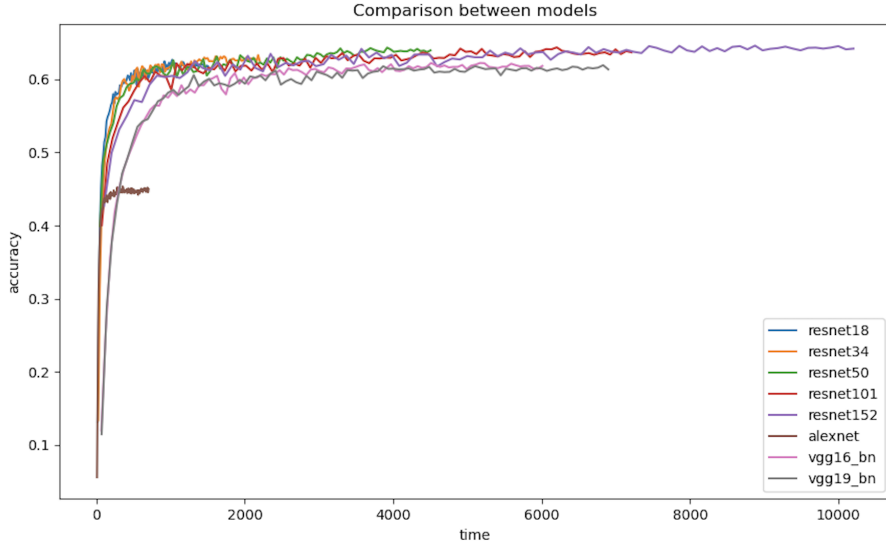


Fig. 5.16: Accuracy achieved by the models over 100 epochs. The x axis is the training time in seconds, while the y axis is the accuracy achieved

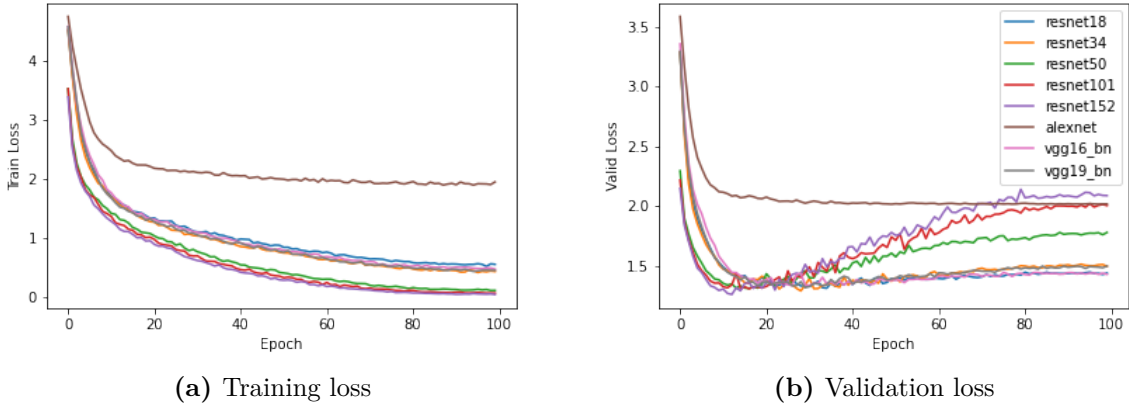


Fig. 5.17: Training loss and validation loss of all models calculated over 100 epochs

As shown in Fig. 5.17a, the train loss decreases at each epoch for each model. For Alexnet, the curve tends to flatten at around 15 epochs, while for the others it flattens at around 60. Rather than observing the training loss trend alone, however, which does not give us the possibility to comprehend correctly the response of the models, we should compare it to the trend of the validation loss shown in Fig. 5.17b. Alexnet remained stable for the duration of the training, with a validation loss comparable to the training loss. The other models, on the other hand, show a rather different behaviour. At around 20 epochs, the validation loss of deeper networks, i.e. Resnet152, Resnet101 and VGG19 starts to increment drastically. For shallower networks of the Resnet architecture, i.e. Resnet18, Resnet34 and Resnet50, and for VGG16 the validation loss decreased for the first 15 epochs and started to increment only after ~40.

In section n. 3.7 we defined over-fitting to be a situation in which the validation loss is much larger than training and from Fig. 5.17b we can see that, although after various numbers of epochs, most of the networks start to enter this condition as the validation loss increases and it becomes much larger than their training loss. We also discussed some

techniques to avoid this, like for e.g. Cross-Validation. For the purpose of this experiment, we only split the dataset 80-20, hence we used no cross-validation or augmentation on the data-set whatsoever.

In this analysis, we can observe the first difference with the results obtained in the first experiment. First of all, the training loss decreases rather slowly when compared to Fig. 5.4 or Fig. 5.8. The validation loss, on the other hand, as we already noticed, increased as the training time increased, while for the other experiment it either remained stable, or increased minimally. To measure inference time, we need to collect a dataset of related pictures, which are not part of the training dataset, to feed to each model. For our tests, we are going to use a data set composed of 200 random pictures. The pictures we are going to use are going to be of different dimensions and different quality in order to see if we can recognize patterns. We can see the results in Fig. 5.18, which displays the training time in milliseconds graphed against the accuracy and the number of epoch used to train. From this figure, we can clearly see that the inference time for every model rarely is measured to be more than 230 milliseconds, with the exception of a few outliers, and most of the models for most epochs have an accuracy between 87% and 92%. In addition, if we analyse the inference time based on the number of epochs (Fig. 5.18b) the models display similar responses.

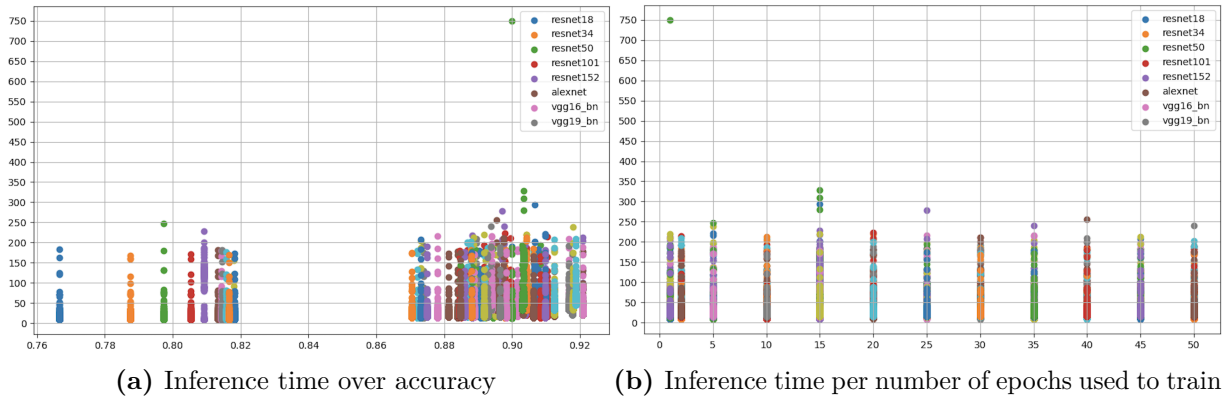


Fig. 5.18: Inference time measured for each model using the 200 pictures dataset discussed previously. The inference time is in milliseconds, while the accuracy for Fig. 5.18a is calculated the percentage of correct predictions over the overall predictions.

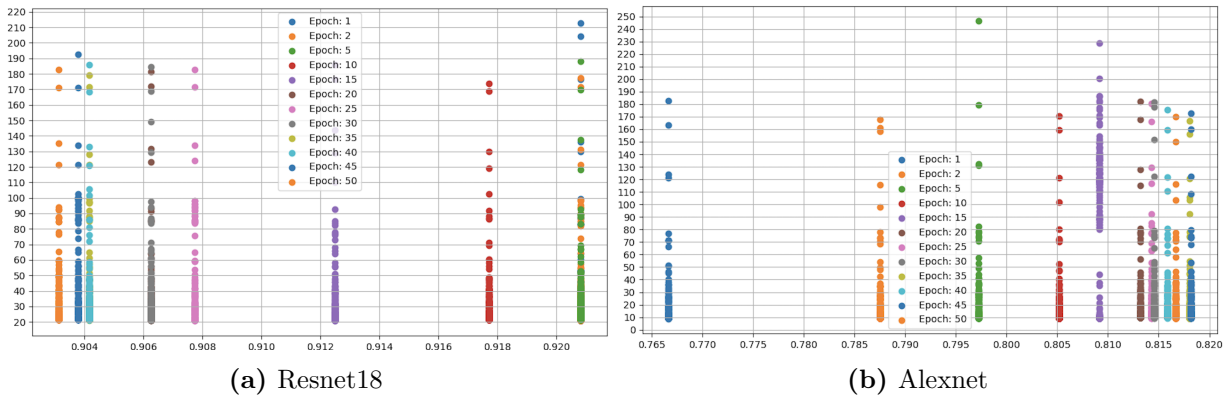


Fig. 5.19: Inference time measured for models Resnet18 and Alexnet

When we compare models individually like in Fig. 5.19, other similarities appear. As a

matter of fact, when we analyse each model, we can observe that some pictures require considerably more time than others. For example, Fig. 5.19 shows the measurements obtained by model Resnet18 (5.19a) and Alexnet (5.19b) and from their response it appears that, at each epoch, there is a constant number of images which takes more time to be processed.

We can run the tool once again to identify the 10 images that took more time to be processed at each epoch, in order to analyse them and find elements which can explain such differences.

The first property of the image we are going to take a look at is the size of the images. Fig. 5.20 shows the results obtained for each model.

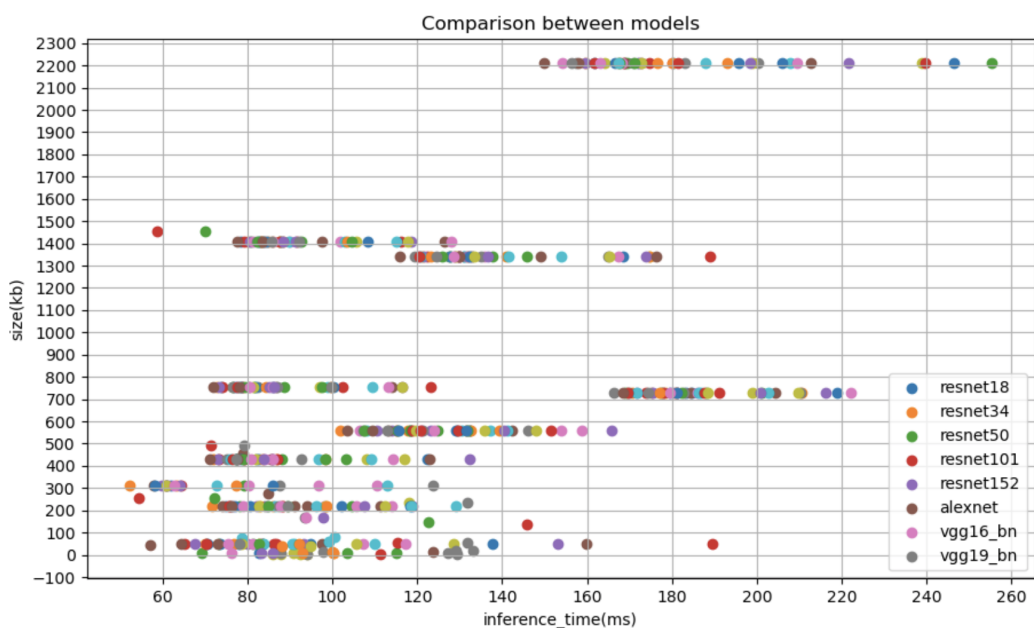


Fig. 5.20: This graph shows the size in kb of the ten slowest images over the time taken to be processed

From the graph we are able to spot some rather interesting behaviours. First of all, we would expect that for each epoch the slowest images would be the same. This hypothesis would be confirmed if the graph showed a group of pictures of the same size having different inference times. However, this is only the case for sizes bigger than 500 kbs. As a matter of fact, we are not able to cluster pictures before 500 kb under a certain inference time range as effectively as we can do for heavier pictures. We can conclude from this that regardless of the amount of training, pictures over 500kb are going to be the slowest ones.

From a closer investigation of the individual models emerged some differences in the response of the single models.

For deeper networks the situation is similar to the discussion we made. As shown in Fig. 5.21, for both Resnet152 and VGG16, the response for pictures smaller than 500kb is noisy, although Resnet152 shows a more stable behaviour than VGG16. This implies that for these networks only the response with images over 500kb displays similarities.

For shallower networks, however, the situation is slightly more different. Fig. 5.22 shows the slowest images identified in the models Resnet18 (Fig. 5.22a) and Alexnet (Fig. 5.22b). Differently from what we concluded before, these models show a much more precise

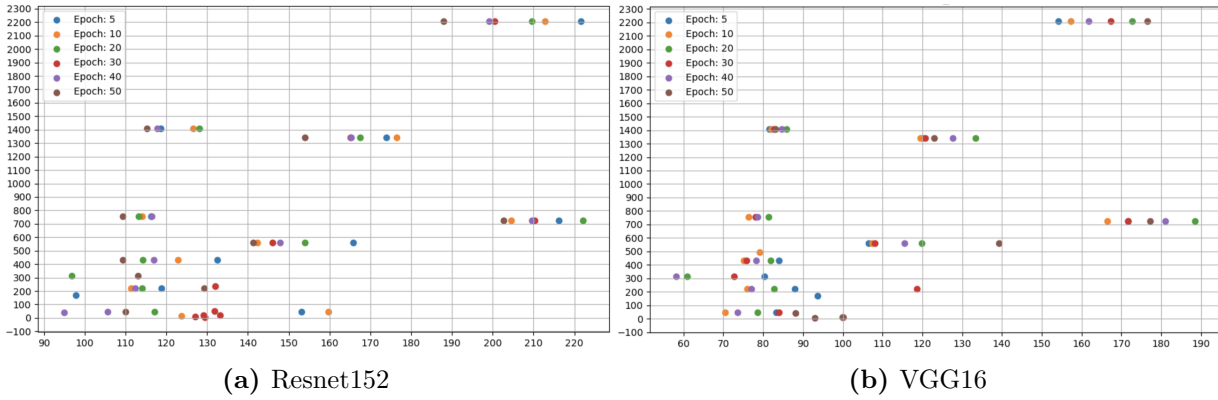


Fig. 5.21: Inference time of the slowest images for models VGG16 and Resnet152

response for images smaller than 500 kb. We are in fact able to cluster the images by size, with the exception of very few outliers. In addition, we can also point out which number of epochs would yield faster predictions for the slowest images. For Resnet18, we can observe that the model trained with 40 epochs is among the fastest for most sizes (with very few exceptions). For Alexnet, on the other hand, the fastest model is the one trained for only 10 epochs. This conclusion, however, does not take into account the accuracy that those models achieved. Using Fig. 5.19a we can see that the same models, i.e. Resnet18 trained with 10 epochs, achieved one of the lowest accuracy rate overall ($\sim 90\%$) and from Fig. 5.19b we can extrapolate a similar conclusion for Alexnet trained with 10 epochs. ($\sim 80\%$). The best trade off between fast inference time and accuracy is achieved when both models have been trained with 50 epochs, however, in case of Resnet18, as we discussed before, this is also the number of epochs in which the validation loss is bigger than the training loss, hence we found ourselves in a situation of slight over-fitting.

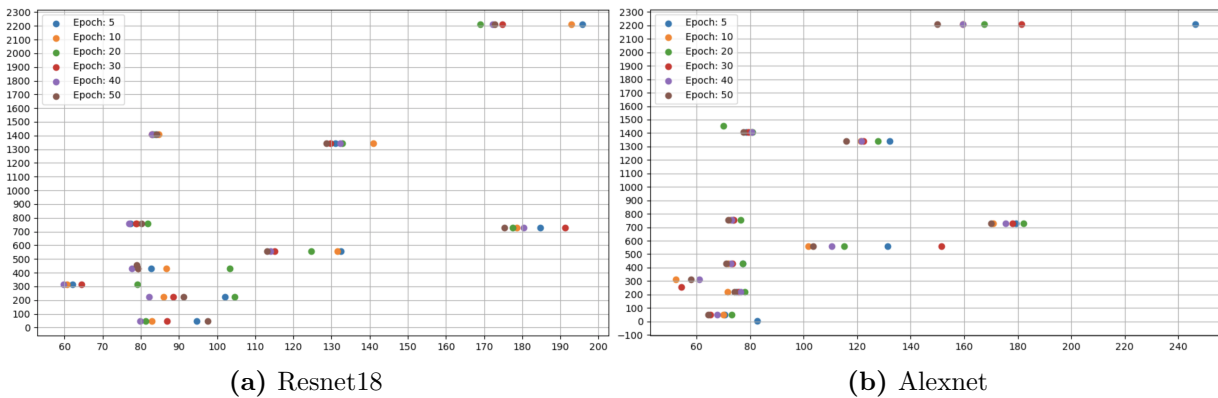


Fig. 5.22: Inference time of the slowest images for models Resnet18 and Alexnet

Regardless of which number of epochs is better for this specific case, the purpose of our exploration is to identify correlation between certain characteristics. From these graphs we are able to find a correlation and to reason about it, in order to tailor future applications. In a real world implementation, if it is known that images with a certain size are going to be among the slowest is useful because it will influence the decision of which hardware to mount on the devices sent to the fields. Additionally, knowing that images with a size of

700 kb are going to take from 200 to 220ms to be classified, will, naturally, help model the time behaviour of these devices and give information to verify that they will not miss any deadline. Furthermore, if we are able to reason about the trade-off between inference time and accuracy, we would also be able to choose a suitable model for different requirements. For example, in applications in which the system needs to respect a hard-deadline, inference time plays a more important role than overall accuracy. By being able to predict both inference time and accuracy from other characteristics, we can find a trade-off which will allow us to respect any hard-deadline.

A closer look to the list of slowest images reveals that there are common pictures amongst all models (Fig. A.1). Using the tool we can investigate if those pictures present similarities that may explain why this is the case. The information collected from the pictures are shown in table 5.8.

Picture n.	Dimensions(x,y)	DPI(x,y)	size(kb)
1	(3888, 2187)	N/A	727
2	(3018, 2585)	(300,300)	2209
3	(3000, 2019)	(300,300)	1341
4	(2003, 2003)	N/A	558
5	(1373, 1012)	(72,72)	1409
6	(2048, 1551)	(300, 300)	221

Table 5.8: Information collected from the slowest pictures

As already demonstrated by Fig. 5.20, each of the five pictures has a size bigger than 500kb, i.e. they are amongst the heaviest pictures on the dataset. Furthermore, they are also amongst the pictures having the highest dimensions. Even though not available for all the pictures, table 5.8 also shows that the pictures have high DPI, which implies that these pictures have very high quality.

Following the calculations we delineated in section 4.2.1, we can hypothesise that images with higher dimensions are more slowly processed by the models. This is due to the fact that each architecture presents pooling layers, which according to equation 4.3, is directly proportional to the dimensions of the images. If we compare Fig. 5.20 and table 5.8, we can also spot a quite interesting relation. For example, if we analyse picture number 6, we can see that it has a size of 221 kb and dimensions of 2048×1551 pixels. According to our hypothesis, we would expect it to be slower than pictures having lower dimensions. However, picture 5, with dimension 1373×1012 pixels, is being processed more slowly or equally by every model at every epoch. We can therefore confute the hypothesis that we just made and conclude that the inference time is influenced not only by the dimension of the images, but also by other characteristics of the images. Studying and analysing these characteristics can produce further results that have not been considered in this paper.

6 Overview and Future Work

Sugar beet plantations, due to their poor performances against other competitors like weed, will benefit from the advancements brought by the introduction of smart farming techniques. Most of the solutions in this field proposed methodologies for increasing production and sustainability based on the recognition and localization of sugar beets using Neural Networks. Neural Networks, however, impose obstacles which, despite their great flexibility, make tailoring applications around them challenging.

In this paper, we investigated how the analysis of the characteristics of Neural Networks brings to find correlations between them that can be used to predict the performances of the networks in a time-wise reliable way.

We started our investigation in chapter 3 by defining which characteristics we were going to use and which could be beneficial in the context of sugar beet recognition. By defining these characteristics, we posed our foundations for the development of the tool which allows for further analysis. To develop this tool, in chapter 4, we explored benchmarking techniques and the characteristics that we would like to have for a correct test environment. With the help of this tool, in chapter 5, we studied two use cases to demonstrate how we can effectively find these correlations and these characteristics, mentioning how they could be used in future applications.

Even though in the two analyses we achieved promising and insightful results, this paper leaves many interrogatives open which need to be explored in future works.

First of all, in chapter 3, we only investigated some of the characteristics which neural networks possess and can be correlated with each other. For example, we did not focus on parameters which influence the performances of the networks, like for e.g. learning rate, batch size or throughput. It is left for further studies to identify other characteristics that can be worth studying to find more correlations.

In chapter 4, only techniques related to measuring execution time have been described. However, benchmarks are also used to measure other metrics, such as energy consumption or memory use. It is left for future work to find better techniques to precisely measure and monitor them, as they are also of the highest importance especially for devices with low on-board resources. Furthermore, in this paper we mainly focused on Linux, therefore purposely neglecting other operating systems, only mentioning some techniques to run benchmarks on mobile devices running Android. The study of measuring techniques for other systems is also left for future work.

In chapter 5, we run the benchmarking tool only on two examples. Even though we obtained promising results, we left some interrogatives behind. Firstly, we only ran the tool with models from three different CNN architectures. Secondly, we did not investigate how ad-hoc-created models will behave under the conditions we defined. Thirdly, the experiments we made have been run without any augmentation or optimization on both the models and datasets. Regarding the datasets used, we only touched the surface regarding image processing and data augmentation. As a matter of fact, we only considered grey-scale

version of the pictures, leaving further analysis for future work. It would be interesting to analyse how the augmentation and modifications of these pictures, like for e.g. blurring, cropping and rotation, will influence the behaviour of the models. Furthermore, it would also be insightful to develop a tool to analyse other characteristics of the images (colour concentration, compression algorithm, etc.) to find correlations between those and inference time. Regarding the models have been trained with the standard batch size, learning rate and were not pre-trained. In addition, they have been trained with full precision. It is left for further investigations to prove if further correlations can be found using different models and different optimizations.

Finally, we only investigated if, and which, correlations can be found studying the performance and the behaviour of neural networks. However, this serves only as a starting point for further applications and we did not investigate if these correlations can be used to optimise real world applications. Further research would be needed to prove it.

The result of our journey poses the first milestone towards the use of characteristics and correlations to make sugar beet recognition more efficient, simpler and more reliable with the hope that it could help to improve production and sustainability of the sugar beet plantations around the world.

References

- [10.16] *RecSys '16: Proceedings of the 10th ACM Conference on Recommender Systems*, New York, NY, USA, 2016. Association for Computing Machinery.
- [AAB⁺15a] Martín Abadi, Ashish Agarwal, Paul Barham, Eugene Brevdo, Zhifeng Chen, Craig Citro, Greg S. Corrado, Andy Davis, Jeffrey Dean, Matthieu Devin, Sanjay Ghemawat, Ian Goodfellow, Andrew Harp, Geoffrey Irving, Michael Isard, Yangqing Jia, Rafal Jozefowicz, Lukasz Kaiser, Manjunath Kudlur, Josh Levenberg, Dandelion Mané, Rajat Monga, Sherry Moore, Derek Murray, Chris Olah, Mike Schuster, Jonathon Shlens, Benoit Steiner, Ilya Sutskever, Kunal Talwar, Paul Tucker, Vincent Vanhoucke, Vijay Vasudevan, Fernanda Viégas, Oriol Vinyals, Pete Warden, Martin Wattenberg, Martin Wicke, Yuan Yu, and Xiaoqiang Zheng. TensorFlow: Large-scale machine learning on heterogeneous systems, 2015. Software available from tensorflow.org.
- [AAB⁺15b] Dario Amodei, Rishita Anubhai, Eric Battenberg, Carl Case, Jared Casper, Bryan Catanzaro, Jingdong Chen, Mike Chrzanowski, Adam Coates, Greg Diamos, Erich Elsen, Jesse Engel, Linxi Fan, Christopher Fougner, Tony Han, Awni Hannun, Billy Jun, Patrick LeGresley, Libby Lin, Sharan Narang, Andrew Ng, Sherjil Ozair, Ryan Prenger, Jonathan Raiman, Sanjeev Satheesh, David Seetapun, Shubho Sengupta, Yi Wang, Zhiqian Wang, Chong Wang, Bo Xiao, Dani Yogatama, Jun Zhan, and Zhenyao Zhu. Deep speech 2: End-to-end speech recognition in english and mandarin, 2015.
- [AAUS⁺19] Muhammad Ayaz, Mohammad Ammad-Uddin, Zubair Sharif, Ali Mansour, and El-Hadi M. Aggoune. Internet-of-Things (IoT)-Based Smart Agriculture: Toward Making the Fields Talk. *IEEE Access*, 7:129551–129583, 2019.
- [AMK16] Bilge Acun, Phil Miller, and Laxmikant Kalé. Variation among processors under turbo boost in hpc systems. pages 1–12, 06 2016.
- [AR20] Saahil Afaq and Smitha Rao. Significance of epochs on training a neural network. *International Journal of Scientific & Technology Research*, 9:485–488, 2020.
- [ARK20] Pranav Adarsh, Pratibha Rathi, and Manoj Kumar. Yolo v3-tiny: Object detection and recognition using one stage improved model. In *2020 6th International Conference on Advanced Computing and Communication Systems (ICACCS)*, pages 687–694, 2020.
- [BC18] Martin Becker and Samarjit Chakraborty. Measuring software performance on linux. *CoRR*, abs/1811.01412, 2018.

- [BCCN18] Simone Bianco, Remi Cadene, Luigi Celona, and Paolo Napoletano. Benchmark analysis of representative deep neural network architectures. *IEEE Access*, 6:64270–64277, 2018.
- [BHC18] M Dian Bah, Adel Hafiane, and Raphael Canals. Deep learning with unsupervised data labeling for weed detection in line crops in uav images. *Remote Sensing*, 10(11), 2018.
- [BLW17] Dirk Beyer, Stefan Löwe, and Philipp Wendler. Reliable benchmarking: requirements and solutions. *International Journal on Software Tools for Technology Transfer*, 21:1–29, 2017.
- [BP20] Tamalika Bhadra and Swapan Paul. Weed management in sugar beet: A review. *Fundamental and Applied Agriculture*, 5(0):1, 2020.
- [BDT⁺16] Mariusz Bojarski, Davide Del Testa, Daniel Dworakowski, Bernhard Firner, Beat Flepp, Prasoon Goyal, Lawrence D. Jackel, Mathew Monfort, Urs Muller, Jiakai Zhang, Xin Zhang, Jake Zhao, and Karol Zieba. End to end learning for self-driving cars, 2016.
- [CBB17] Qingqing Cao, Niranjan Balasubramanian, and Aruna Balasubramanian. Mobirnn: Efficient recurrent neural network execution on mobile gpu. In *Proceedings of the 1st International Workshop on Deep Learning for Mobile Systems and Applications*, EMDL ’17, page 1–6, New York, NY, USA, 2017. Association for Computing Machinery.
- [CCG17] Emine Cengil, Ahmet Cinar, and Zafer Gueler. A gpu-based convolutional neural network approach for image classification. In *2017 International Artificial Intelligence and Data Processing Symposium (IDAP)*, pages 1–6, 2017.
- [CM10] Franco Cioni and Gianfranco Maines. Weed Control in Sugarbeet. *Sugar Tech*, 12(3-4):243–255, December 2010.
- [CPC16] Alfredo Canziani, Adam Paszke, and Eugenio Culurciello. An analysis of deep neural network models for practical applications. *CoRR*, abs/1605.07678, 2016.
- [Der16] Leon Derczynski. Complementarity, F-score, and NLP evaluation. In *Proceedings of the Tenth International Conference on Language Resources and Evaluation (LREC’16)*, pages 261–266, Portorož, Slovenia, May 2016. European Language Resources Association (ELRA).
- [DHH⁺18] J. Duarte, S. Han, P. Harris, S. Jindariani, E. Kreinar, B. Kreis, J. Ngadiuba, M. Pierini, R. Rivera, N. Tran, and Z. Wu. Fast inference of deep neural networks in FPGAs for particle physics. *Journal of Instrumentation*, 13(07):P07027–P07027, jul 2018.
- [Die95] Tom Dietterich. Overfitting and undercomputing in machine learning. *ACM computing surveys (CSUR)*, 27(3):326–327, 1995.

- [DSSM09] Eulanda M. Dos Santos, Robert Sabourin, and Patrick Maupin. Overfitting cautious selection of classifier ensembles with genetic algorithms. *Inf. Fusion*, 10(2):150–162, apr 2009.
- [fas21] fast.ai. Fastai documentation. <https://docs.fast.ai/>, Nov 29, 2021. [Online; accessed 27-12-2021].
- [FHZ93] William Finnoff, Ferdinand Hergert, and Hans Georg Zimmermann. Improving model selection by nonconvergent methods. *Neural Networks*, 6(6):771–783, 1993.
- [FMF⁺14] C. Frasconi, L. Martelloni, M. Fontanelli, M. Raffaelli, L. Emmi, Michel Pirchio, and A. Peruzzi. Design and full realization of physical weed control (PWC) automated machine within the RHEA project. 2014.
- [GBC16] Ian Goodfellow, Yoshua Bengio, and Aaron Courville. *Deep Learning*. MIT Press, 2016. <http://www.deeplearningbook.org>.
- [GDDM14] Ross Girshick, Jeff Donahue, Trevor Darrell, and Jitendra Malik. Rich feature hierarchies for accurate object detection and semantic segmentation. 2014.
- [GDP09] Alexander Guzhva, Sergey Dolenko, and Igor Persiantsev. Multifold acceleration of neural network computations using gpu. In Cesare Alippi, Marios Polycarpou, Christos Panayiotou, and Georgios Ellinas, editors, *Artificial Neural Networks – ICANN 2009*, pages 373–380, Berlin, Heidelberg, 2009. Springer Berlin Heidelberg.
- [Gei21] Amnon Geifman. The correct way to measure inference time of deep neural networks, 2021.
- [GFP⁺20] Junfeng Gao, Andrew P. French, Michael P. Pound, Yong He, Tony P. Pridmore, and Jan G. Pieters. Deep convolutional neural networks for image-based *Convolvulus sepium* detection in sugar beet fields. *Plant Methods*, 16(1):29, December 2020.
- [GIC20] Dimitrios Glaroudis, Athanasios Iossifides, and Periklis Chatzimisios. Survey, comparison and research challenges of IoT application protocols for smart farming. *Computer Networks*, 168:107037, February 2020.
- [GJJ⁺17] Thomas Mosgaard Giselsson, Rasmus Nyholm Jørgensen, Peter Kryger Jensen, Mads Dyrmann, and Henrik Skov Midtiby. A public image database for benchmark of plant seedling classification algorithms, 2017.
- [Goo10] Google. Machine learning crash course. <https://developers.google.com/machine-learning/crash-course/classification/accuracy>, 2020-02-10. [Online; accessed 27-12-2021].
- [GTA⁺21] Jakob Gawlikowski, Cedrique Rovile Njieutcheu Tassi, Mohsin Ali, Jongseok Lee, Matthias Humt, Jianxiang Feng, Anna Kruspe, Rudolph Triebel, Peter Jung, Ribana Roscher, Muhammad Shahzad, Wen Yang, Richard Bamler, and Xiao Xiang Zhu. A survey of uncertainty in deep neural networks, 2021.

- [HD19] Dan Hendrycks and Thomas Dietterich. Benchmarking neural network robustness to common corruptions and perturbations, 2019.
- [HEKK19] Sara Hooker, Dumitru Erhan, Pieter-Jan Kindermans, and Been Kim. A benchmark for interpretability methods in deep neural networks, 2019.
- [HG20] Jeremy Howard and Sylvain Gugger. Fastai: A layered api for deep learning. *Information*, 11(2), 2020.
- [HLM⁺16] Song Han, Xingyu Liu, Huizi Mao, Jing Pu, Ardavan Pedram, Mark A. Horowitz, and William J. Dally. Eie: Efficient inference engine on compressed deep neural network, 2016.
- [HM13] Haibo He and Yunqian Ma. *Imbalanced Learning: Foundations, Algorithms, and Applications*. Wiley-IEEE Press, 1st edition, 2013.
- [HSHK21] Denis Huseljic, Bernhard Sick, Marek Herde, and Daniel Kottke. Separation of aleatoric and epistemic uncertainty in deterministic deep neural networks. In *2020 25th International Conference on Pattern Recognition (ICPR)*, pages 9172–9179, 2021.
- [HW20] Ramy Hussein and Rabab Ward. Chapter 4 - energy-efficient eeg monitoring systems for wireless epileptic seizure detection. pages 69–85, 2020.
- [HW21] Eyke Hüllermeier and Willem Waegeman. Aleatoric and epistemic uncertainty in machine learning: an introduction to concepts and methods. *Machine Learning*, 110, 03 2021.
- [HWT⁺15] Brody Huval, Tao Wang, Sameep Tandon, Jeff Kiske, Will Song, Joel Pazhayampallil, Mykhaylo Andriluka, Pranav Rajpurkar, Toki Migimatsu, Royce Cheng-Yue, Fernando Mujica, Adam Coates, and Andrew Y. Ng. An empirical evaluation of deep learning on highway driving, 2015.
- [HZRS14] Kaiming He, Xiangyu Zhang, Shaoqing Ren, and Jian Sun. Spatial pyramid pooling in deep convolutional networks for visual recognition. *Lecture Notes in Computer Science*, page 346–361, 2014.
- [HZRS15] Kaiming He, Xiangyu Zhang, Shaoqing Ren, and Jian Sun. Deep residual learning for image recognition. *CoRR*, abs/1512.03385, 2015.
- [IRP⁺21] Nahina Islam, Md Mamunur Rashid, Faezeh Pasandideh, Biplob Ray, Steven Moore, and Rajan Kadel. A Review of Applications and Communication Technologies for Internet of Things (IoT) and Unmanned Aerial Vehicle (UAV) Based Sustainable Smart Farming. *Sustainability*, 13(4):1821, February 2021.
- [IS15] Sergey Ioffe and Christian Szegedy. Batch normalization: Accelerating deep network training by reducing internal covariate shift. 2015.
- [ITK⁺19] Andrey Ignatov, Radu Timofte, Andrei Kulik, Seungsoo Yang, Ke Wang, Felix Baum, Max Wu, Lirong Xu, and Luc Van Gool. Ai benchmark: All about deep learning on smartphones in 2019, 2019.

- [JK15] H. Jabbar and Rafiqul Zaman Khan. Methods to avoid over-fitting and under-fitting in supervised machine learning (comparative study). *Computer Science, Communication and Instrumentation Devices*, pages 163–172, 2015.
- [KD09] Armen Der Kiureghian and Ove Ditlevsen. Aleatory or epistemic? does it matter? *Structural Safety*, 31(2):105–112, 2009. Risk Acceptance and Risk Communication.
- [Ker10] Michael Kerrisk. *The Linux Programming Interface: A Linux and UNIX System Programming Handbook*. No Starch Press, USA, 1st edition, 2010.
- [Ker21] Michael Kerrisk. Linux manual page, 2021.
- [KG17] Alex Kendall and Yarin Gal. What uncertainties do we need in bayesian deep learning for computer vision? *CoRR*, abs/1703.04977, 2017.
- [KRKP⁺16] Thomas Kluyver, Benjamin Ragan-Kelley, Fernando Pérez, Brian Granger, Matthias Bussonnier, Jonathan Frederic, Kyle Kelley, Jessica Hamrick, Jason Grout, Sylvain Corlay, Paul Ivanov, Damián Avila, Safia Abdalla, and Carol Willing. Jupyter notebooks – a publishing format for reproducible computational workflows. In F. Loizides and B. Schmidt, editors, *Positioning and Power in Academic Publishing: Players, Agents and Agendas*, pages 87 – 90. IOS Press, 2016.
- [KSH12] Alex Krizhevsky, Ilya Sutskever, and Geoffrey E Hinton. Imagenet classification with deep convolutional neural networks. In F. Pereira, C. J. C. Burges, L. Bottou, and K. Q. Weinberger, editors, *Advances in Neural Information Processing Systems*, volume 25. Curran Associates, Inc., 2012.
- [LHS⁺16a] P. Lottes, M. Hoeferlin, S. Sander, M. Müter, P. Schulze, and Lammers C. Stachniss. An effective classification system for separating sugar beets and weeds for precision farming applications. In *2016 IEEE International Conference on Robotics and Automation (ICRA)*, pages 5157–5163, Stockholm, Sweden, May 2016. IEEE.
- [LHS⁺16b] P. Lottes, M. Hoeferlin, S. Sander, M. Müter, P. Schulze, and Lammers C. Stachniss. An effective classification system for separating sugar beets and weeds for precision farming applications. In *2016 IEEE International Conference on Robotics and Automation (ICRA)*, pages 5157–5163, 2016.
- [LHZ⁺20] Chunjie Luo, Xiwen He, Jianfeng Zhan, Lei Wang, Wanling Gao, and Jiahui Dai. Comparison and benchmarking of ai models and frameworks on mobile devices, 2020.
- [Luc22] Brodo Luca. Weed management in sugar beet farms: Quo vadis? unpublished, 2022.
- [LY20] Yuzhen Lu and Sierra Young. A survey of public datasets for computer vision tasks in precision agriculture. *Computers and Electronics in Agriculture*, 178:105760, November 2020.

- [Mas91] Amédée Masclef. Sugar Beet, 1891.
- [May03] M J May. Economic consequences for UK farmers of growing GM herbicide tolerant sugar beet. *Annals of Applied Biology*, 142(1):41–48, February 2003.
- [Mit97] Tom M Mitchell. *Machine Learning*. New York McGraw-Hill, 1997.
- [MLS17] Andres Milioto, Philipp Lottes, and Cyrill Stachniss. Real-time blob-wise sugar beets vs weeds classification for monitoring fields using convolutional neural networks. *ISPRS Annals of Photogrammetry, Remote Sensing & Spatial Information Sciences*, 4, 2017.
- [MPSG21] Jannis Machleb, Gerassimos G. Petrinatos, Markus Sökefeld, and Roland Gerhards. Sensor-Based Intrarow Mechanical Weed Control in Sugar Beets with Motorized Finger Weeder. *Agronomy*, 11(8):1517, July 2021.
- [MTK⁺17] Pavlo Molchanov, Stephen Tyree, Tero Karras, Timo Aila, and Jan Kautz. Pruning convolutional neural networks for resource efficient inference, 2017.
- [Mur16] John Murphy. An overview of convolutional neural network architectures for deep learning. *Microway Inc*, 2016.
- [NWH21] Abozar Nasirahmadi, Ulrike Wilczek, and Oliver Hensel. Sugar beet damage detection during harvesting using different convolutional neural network models. *Agriculture*, 11(11), 2021.
- [NYC15] Anh Nguyen, Jason Yosinski, and Jeff Clune. Deep neural networks are easily fooled: High confidence predictions for unrecognizable images, 2015.
- [OFR⁺19] Yaniv Ovadia, Emily Fertig, Jie Ren, Zachary Nado, D Sculley, Sebastian Nowozin, Joshua V. Dillon, Balaji Lakshminarayanan, and Jasper Snoek. Can you trust your model’s uncertainty? evaluating predictive uncertainty under dataset shift, 2019.
- [OJ04] Kyoung-Su Oh and Keechul Jung. Gpu implementation of neural networks. *Pattern Recognition*, 37(6):1311–1314, 2004.
- [PE89] Perugini and Engeler. Neural network learning time: effects of network and training set size. In *International 1989 Joint Conference on Neural Networks*, pages 395–401 vol.2, 1989.
- [Pet04] J. Petersen. A Review on Weed Control in Sug- arbeet. *Inderjit (Ed), Weed Biology and Management.*, 2004.
- [PJVY⁺13] Thomas Paine, Hailin Jin, Jianchao Yang, Zhe Lin, and Thomas Huang. Gpu asynchronous stochastic gradient descent to speed up neural network training, 2013.
- [Pre00] Lutz Prechelt. Early stopping - but when? 03 2000.
- [PVZJ12] Omkar M. Parkhi, Andrea Vedaldi, Andrew Zisserman, and C. V. Jawahar. Cats and dogs. In *IEEE Conference on Computer Vision and Pattern Recognition*, 2012.

- [RAMP20] W. Ramirez, P. Achancaray, L. F. Mendoza, and M. A. C. Pacheco. DEEP CONVOLUTIONAL NEURAL NETWORKS FOR WEED DETECTION IN AGRICULTURAL CROPS USING OPTICAL AERIAL IMAGES. *The International Archives of the Photogrammetry, Remote Sensing and Spatial Information Sciences*, XLII-3/W12-2020:551–555, November 2020.
- [RCK⁺20] Vijay Janapa Reddi, Christine Cheng, David Kanter, Peter Mattson, Guenther Schmuelling, Carole-Jean Wu, Brian Anderson, Maximilien Breughe, Mark Charlebois, William Chou, Ramesh Chukka, Cody Coleman, Sam Davis, Pan Deng, Greg Diamos, Jared Duke, Dave Fick, J. Scott Gardner, Itay Hubara, Sachin Idgunji, Thomas B. Jablin, Jeff Jiao, Tom St. John, Pankaj Kanwar, David Lee, Jeffery Liao, Anton Lokhmotov, Francisco Massa, Peng Meng, Paulius Micikevicius, Colin Osborne, Gennady Pekhimenko, Arun Tejasve Raghunath Rajan, Dilip Sequeira, Ashish Sirasao, Fei Sun, Hanlin Tang, Michael Thomson, Frank Wei, Ephrem Wu, Lingjie Xu, Koichi Yamada, Bing Yu, George Yuan, Aaron Zhong, Peizhao Zhang, and Yuchen Zhou. Mlperf inference benchmark, 2020.
- [RDS⁺14] Olga Russakovsky, Jia Deng, Hao Su, Jonathan Krause, Sanjeev Satheesh, Sean Ma, Zhiheng Huang, Andrej Karpathy, Aditya Khosla, Michael S. Bernstein, Alexander C. Berg, and Li Fei-Fei. Imagenet large scale visual recognition challenge. *CoRR*, abs/1409.0575, 2014.
- [RDS⁺15] Olga Russakovsky, Jia Deng, Hao Su, Jonathan Krause, Sanjeev Satheesh, Sean Ma, Zhiheng Huang, Andrej Karpathy, Aditya Khosla, Michael Bernstein, Alexander C. Berg, and Li Fei-Fei. ImageNet Large Scale Visual Recognition Challenge. *International Journal of Computer Vision (IJCV)*, 115(3):211–252, 2015.
- [RGC⁺16] Minsoo Rhu, Natalia Gimelshein, Jason Clemons, Arslan Zulfiqar, and Stephen W. Keckler. vdnn: Virtualized deep neural networks for scalable, memory-efficient neural network design, 2016.
- [RM99] Russell D Reed and Robert J Marks. *Neural smithing supervised learning in feedforward artificial neural networks*. 1999. OCLC: 1227498094.
- [RNSF20] Rekha Raja, Thuy T. Nguyen, David C. Slaughter, and Steven A. Fennimore. Real-time robotic weed knife control system for tomato and lettuce based on geometric appearance of plant labels. *Biosystems Engineering*, 194:152–164, June 2020.
- [Rud17] Sebastian Ruder. An overview of gradient descent optimization algorithms, 2017.
- [SD89] EE Schweizer and A.G Dexter. "Weed control in sugarbeets (*Beta vulgaris*) in North America". 1989.
- [SGSS16] Arti Singh, Baskar Ganapathysubramanian, Asheesh Kumar Singh, and Soumik Sarkar. Machine Learning for High-Throughput Stress Phenotyping in Plants. *Trends in Plant Science*, 21(2):110–124, 2016.

- [SIHvH18] Hyun K. Suh, Joris IJsselmuiden, Jan Willem Hofstee, and Eldert J. van Henten. Transfer learning for the classification of sugar beet and volunteer potato under field conditions. *Biosystems Engineering*, 174:50–65, October 2018.
- [SJS06] Marina Sokolova, Nathalie Japkowicz, and Stan Szpakowicz. Beyond accuracy, f-score and roc: A family of discriminant measures for performance evaluation. volume Vol. 4304, pages 1015–1021, 01 2006.
- [SKD19] Kyoung Song, Myeongchan Kim, and Synho Do. The latest trends in the use of deep learning in radiology illustrated through the stages of deep learning algorithm development. *Journal of the Korean Society of Radiology*, 80:202, 03 2019.
- [SLJ⁺14] Christian Szegedy, Wei Liu, Yangqing Jia, Pierre Sermanet, Scott Reed, Dragomir Anguelov, Dumitru Erhan, Vincent Vanhoucke, and Andrew Rabinovich. Going deeper with convolutions, 2014.
- [Smi18] Leslie N. Smith. A disciplined approach to neural network hyper-parameters: Part 1 - learning rate, batch size, momentum, and weight decay. *CoRR*, abs/1803.09820, 2018.
- [ST17] Leslie N. Smith and Nicholay Topin. Super-convergence: Very fast training of residual networks using large learning rates. *CoRR*, abs/1708.07120, 2017.
- [Ste01] David B. Stewart. Measuring execution time and real-time performance. 2001.
- [Suh18] Hyun Suh. *Advanced classification of volunteer potato in a sugar beet field*. PhD thesis, 01 2018.
- [SZ15] Karen Simonyan and Andrew Zisserman. Very deep convolutional networks for large-scale image recognition, 2015.
- [TLZ⁺19] Nesime Tatbul, Tae Jun Lee, Stan Zdonik, Mejbah Alam, and Justin Gottschlich. Precision and recall for time series, 2019.
- [TMK16] Surat Teerapittayanon, Bradley McDanel, and H.T. Kung. Branchynet: Fast inference via early exiting from deep neural networks. In *2016 23rd International Conference on Pattern Recognition (ICPR)*, pages 2464–2469, 2016.
- [UKG⁺20] Thomas Unterthiner, Daniel Keysers, Sylvain Gelly, Olivier Bousquet, and Ilya O. Tolstikhin. Predicting neural network accuracy from weights. *ArXiv*, abs/2002.11448, 2020.
- [UKG⁺21] Thomas Unterthiner, Daniel Keysers, Sylvain Gelly, Olivier Bousquet, and Ilya Tolstikhin. Predicting neural network accuracy from weights, 2021.
- [vKAH⁺15] Jóakim von Kistowski, Jeremy Arnold, Karl Huppler, Klaus-Dieter Lange, John Henning, and Paul Cao. How to build a benchmark. 02 2015.

- [vR74] C. J. van Rijsbergen. Foundation of evaluation. *Journal of Documentation*, 30:365–373, 1974.
- [WDESP17] Peter Wägemann, Tobias Distler, Christian Eichler, and Wolfgang Schröder-Preikschat. Benchmark generation for timing analysis. In *2017 IEEE Real-Time and Embedded Technology and Applications Symposium (RTAS)*, pages 319–330, 2017.
- [YKU⁺20] Jinhui Yi, Lukas Krusenbaum, Paula Unger, Hubert Hüging, Sabine J. Seidel, Gabriel Schaaf, and Juergen Gall. Deep learning for non-invasive diagnosis of nutrient deficiencies in sugar beet using rgb images. *Sensors*, 20(20), 2020.
- [YNDT18] Rikiya Yamashita, Mizuho Nishio, Richard Do, and Kaori Togashi. Convolutional neural networks: an overview and application in radiology. *Insights into Imaging*, 9, 06 2018.
- [ZAZ⁺18] Hongyu Zhu, Mohamed Akrout, Bojian Zheng, Andrew Pelegris, Anand Jayarajan, Amar Phanishayee, Bianca Schroeder, and Gennady Pekhimenko. Benchmarking and analyzing deep neural network training. In *2018 IEEE International Symposium on Workload Characterization (IISWC)*, pages 88–100, 2018.
- [ZS21] Gennady Fedorov Shaojuan Zhu and Abhinav Singh. Intel® oneapi math kernel library (onemkl) benchmarks suite, 2021.

A Appendix

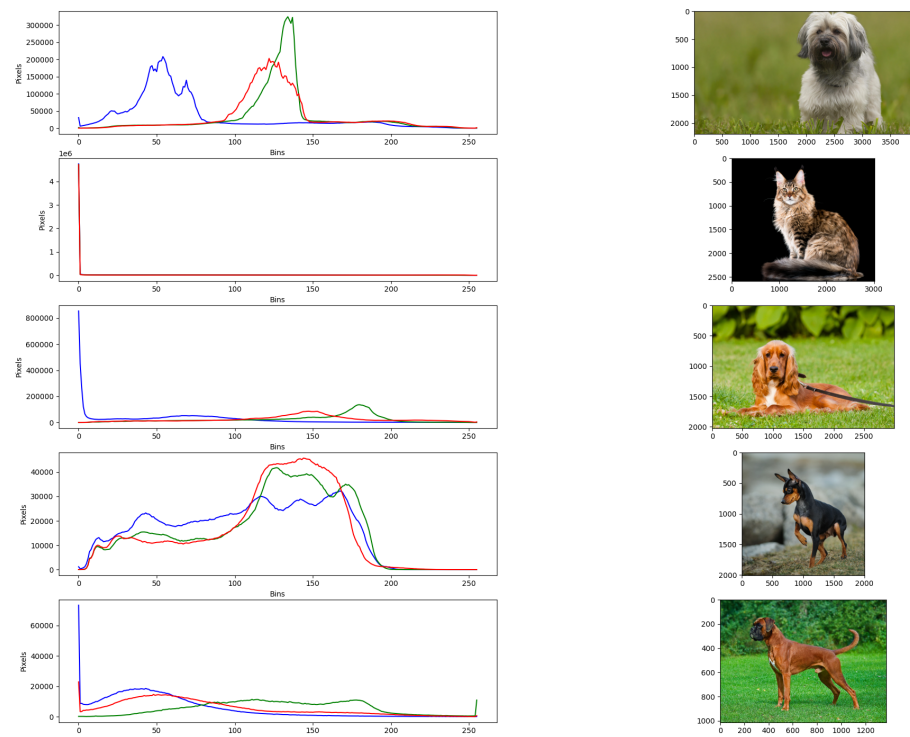


Fig. A.1: Histogram of the slowest files in common amongst all models

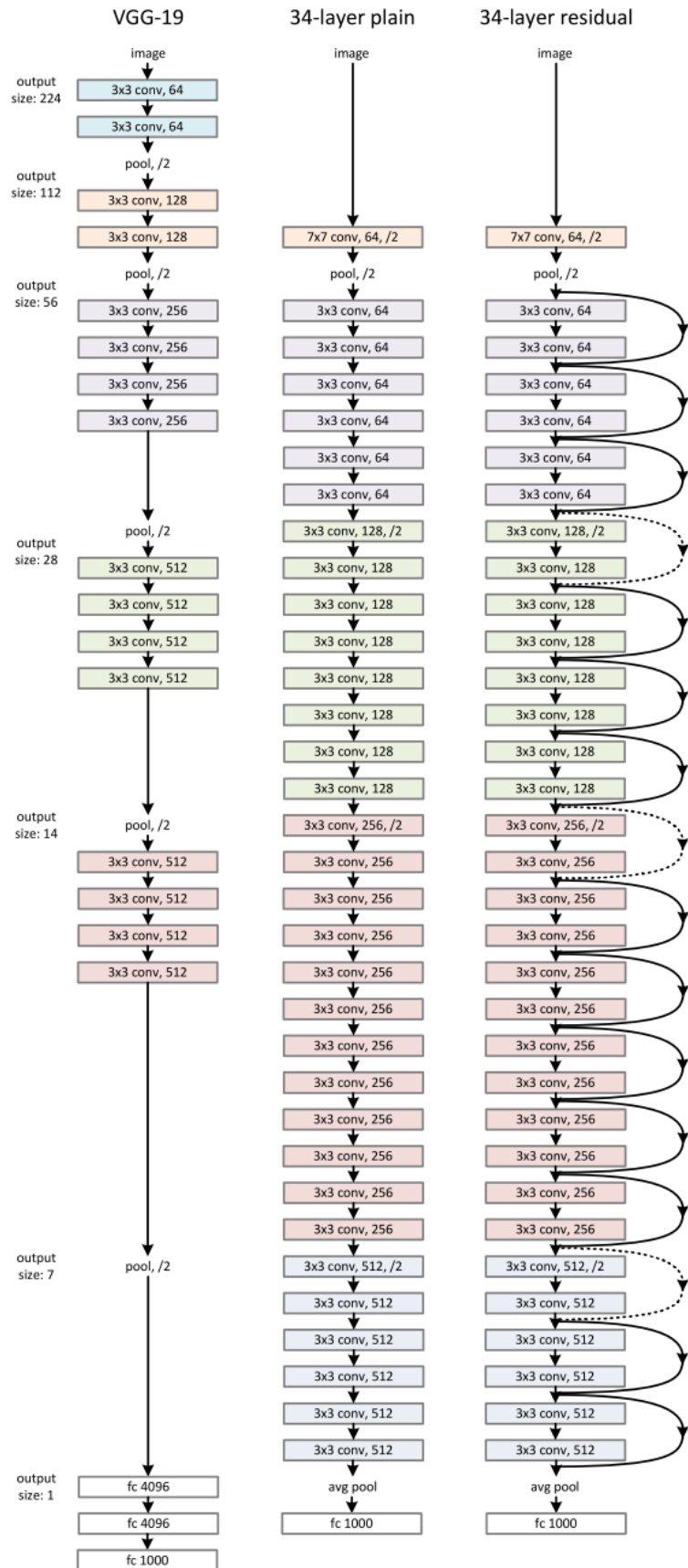


Fig. A.2: Left: the VGG-19 model [41] (19.6 billion FLOPs) as a reference. Middle: a plain network with 34 parameter layers (3.6 billion FLOPs). Right: a residual network with 34 parameter layers (3.6 billion FLOPs). The dotted shortcuts increase dimensions. [HZRS15]

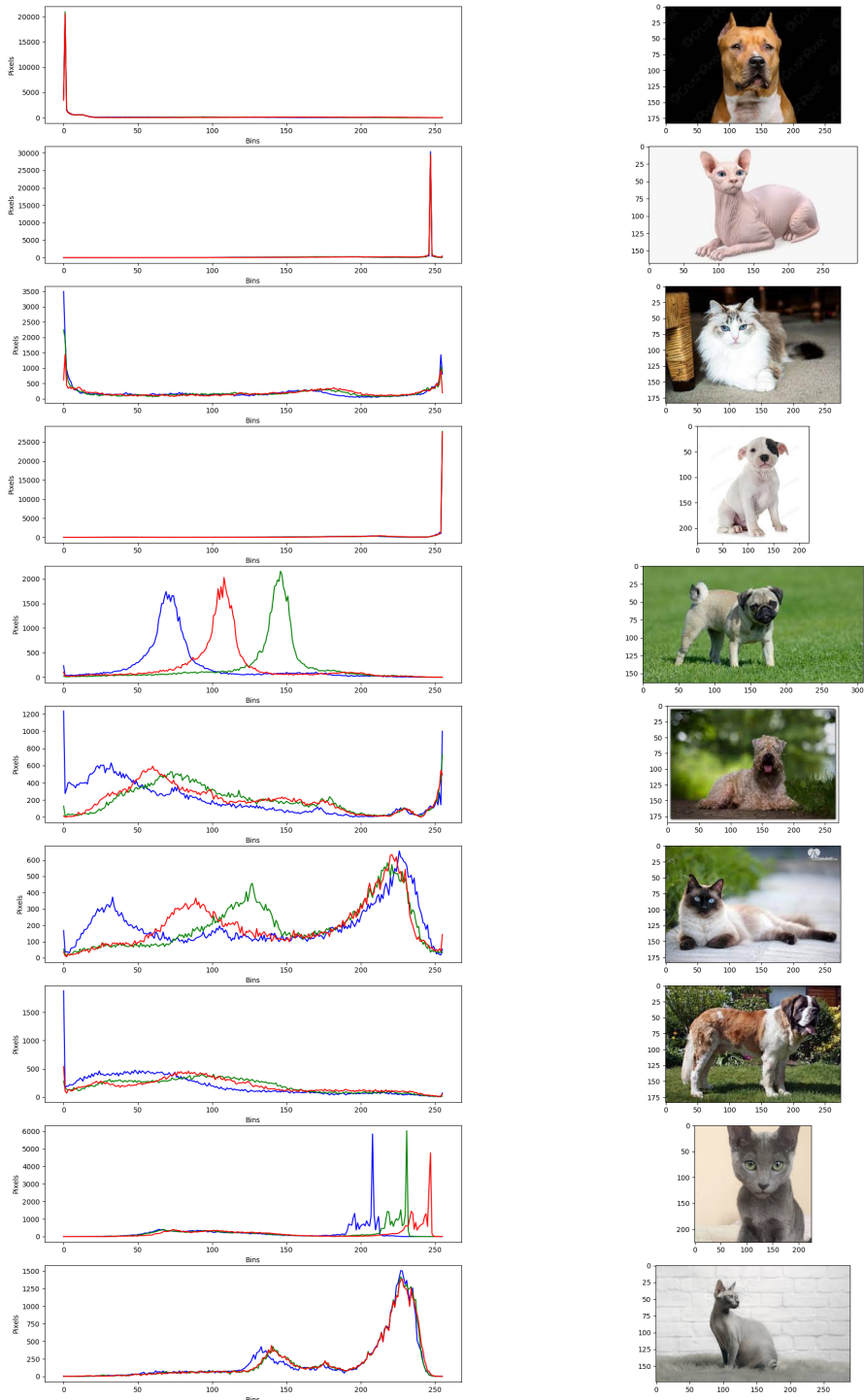


Fig. A.3: Histogram of the fastest files of Resnet 152

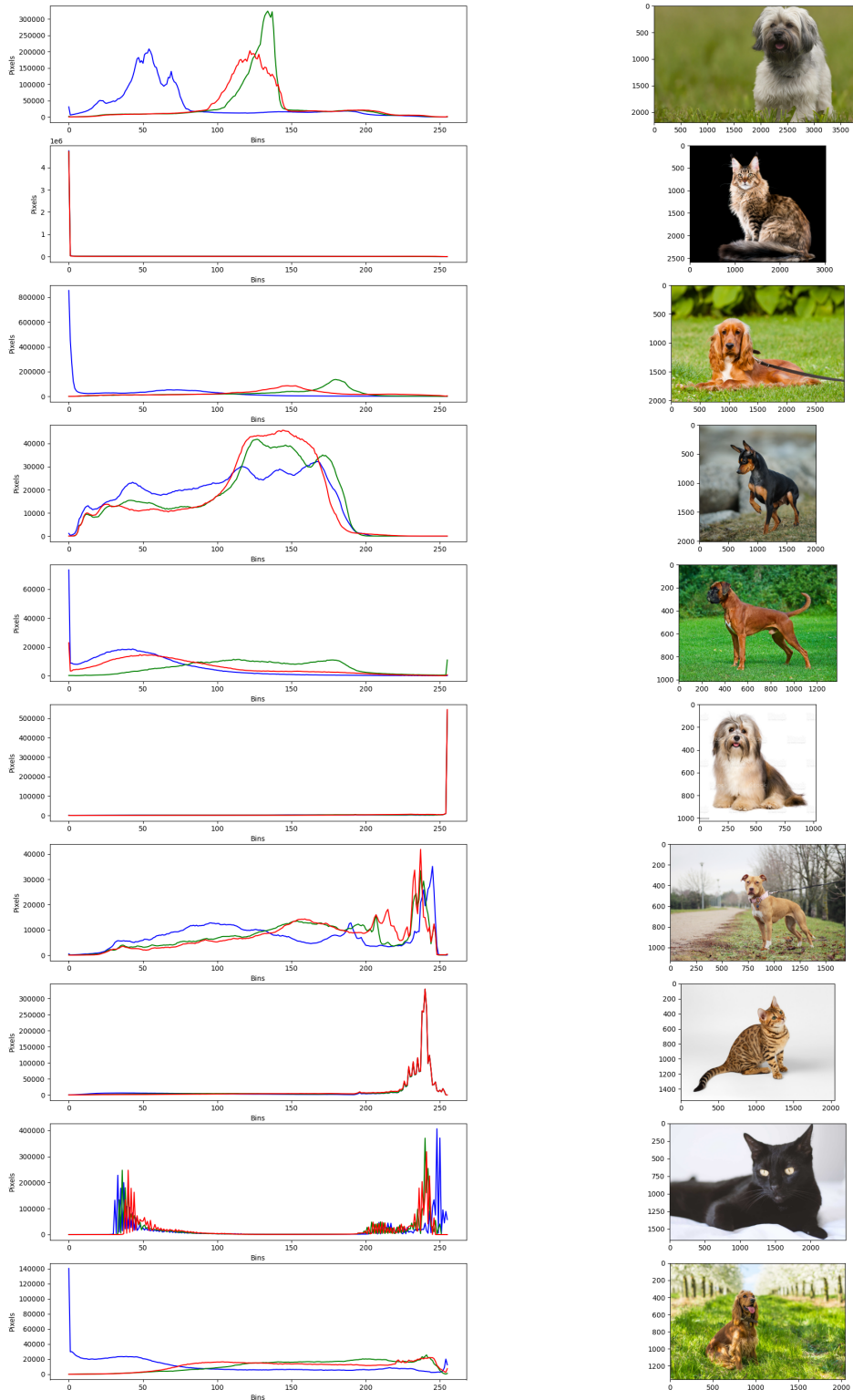


Fig. A.4: Histogram of the slowest files of Resnet152



Fig. A.5: Complete result of the test for inference time in the seedlings dataset



Fig. A.6: Complete result of the test for inference time in the seedlings dataset with grey images



Fig. A.7: Complete result of the test for inference time in the seedlings dataset with grey images.
The inference here is calculated by feeding grey scale images to the models